The *Drosophila* dystonia gene homolog *Neurocalcin* facilitates sleep by inhibiting a movement-promoting neural network

Ko-Fan Chen, Angélique Lamaze, Patrick Krätschmer and James E.C. Jepson*

Department of Experimental and Clinical Epilepsy, UCL Institute of Neurology, UK

*Correspondence to: j.jepson@ucl.ac.uk

Abstract

Primary dystonia is a hyperkinetic movement disorder linked to altered dopaminergic signaling and synaptic plasticity in regions of the brain involved in motor control. Mutations in *HPCA*, encoding the neuronal calcium sensor Hippocalcin, are associated with primary dystonia, suggesting a function for Hippocalcin in regulating the initiation and/or maintenance of activity. However, such a role for Hippocalcin or Hippocalcin homologs has yet to be demonstrated in vivo. Here we investigate the cellular and organismal functions of the *Drosophila* Hippocalcin homolog Neurocalcin (NCA), and define a role for NCA in promoting sleep by suppressing nighttime hyperactivity. We show that NCA acts in a common pathway with the D1-type Dop1R1 dopamine receptor and facilitates sleep by inhibiting neurotransmitter release from a multi-component activity-promoting circuit. Our results suggest conserved roles for Hippocalcin homologs in modulating motor control through dopaminergic pathways, suppressing aberrant movements in humans and inappropriate nighttime locomotion in *Drosophila*.

23 **Introduction**

24 Primary dystonia is characterized by repetitive involuntary movements or sustained
25 abnormal postures, and represents the third most common movement disorder after
26 benign tremor and Parkinson's disease (Fahn, 1988; Wenning et al., 2005). Dystonia
27 has been linked to altered neurotransmission and/or plasticity of circuits within the
28 basal ganglia, a group of nuclei involved in action initiation and maintenance, as well
29 as associated inputs/outputs (Calabresi et al., 2016; Karimi and Perlmutter, 2015;
30 Pappas et al., 2015; Weisheit and Dauer, 2015). However, the molecular pathways
31 underlying this disorder remain unclear.

32 Identifying genetic loci linked to hereditary forms of primary dystonia
33 represents a useful strategy to uncover such pathways. Mutations in *GNAL*, encoding
34 $G\alpha_{olf}$, have been linked to primary dystonia (Fuchs et al., 2013), and since the $G\alpha_{olf}$
35 G-protein α-subunit couples to D1-type dopamine receptors, this finding supports a
36 link between dystonia and altered dopaminergic signaling (Karimi and Perlmutter,
37 2015). Indeed, current models suggest that the basal ganglia regulate motor control
38 through two distinct circuits, the direct and indirect pathways, that are defined by
39 expression of D1- and D2-type type dopamine receptors respectively (Gerfen and
40 Surmeier, 2011; Tecuapetla et al., 2016). These pathways antagonistically influence
41 activity of large-scale brain networks (Lee et al., 2016), and an imbalance of direct
42 versus indirect pathway signaling has been proposed to cause dystonia (Breakefield et
43 al., 2008; Peterson et al., 2010; Tanabe et al., 2009; Yokoi et al., 2015). Mutations in
44 *dTorsin*, the *Drosophila* homolog of the dystonia gene *TOR1A*, reduce dopamine
45 levels by suppressing expression of the dopamine synthesis factor GTP
46 cyclohydrolase (Wakabayashi-Ito et al., 2015; Wakabayashi-Ito et al., 2011), further
47 linking dystonia to altered dopamine signaling.

Recent studies have identified an array of further loci linked to primary dystonia, including *THAP1*, *ANO3*, *KCTD17* and *HPCA* (Charlesworth et al., 2015; Charlesworth et al., 2012; Fuchs et al., 2009; Mencacci et al., 2015). However, in vivo data linking these genes to motor control and/or dopaminergic pathways is limited. Interestingly, mutations in the *Drosophila KCTD17* homologue *insomniac* result in reduced sleep (i.e increased movement), a phenotype that can be rescued by inhibiting dopamine synthesis (Pfeiffenberger and Allada, 2012; Stavropoulos and Young, 2011). Thus, we sought to examine whether other dystonia gene homologs in *Drosophila* also impacted sleep, beginning with the *Drosophila HPCA* homolog *Neurocalcin* (*Nca*).

NCA and Hippocalcin (the *HPCA* gene product) act as neuronal calcium sensors, cytoplasmic proteins that bind to calcium via EF hand domains and translocate to lipid membranes through a calcium-dependent myristoylation switch (Burgoyne and Haynes, 2012). This switch modulates interactions with membrane-bound ion channels and receptors, altering target function or localization (Braunewell and Klein-Szanto, 2009; Burgoyne and Haynes, 2012). Missense mutations in *HPCA* have been linked to DYT2 primary isolated dystonia, which predominantly affects the upper limbs, cervical and cranial regions (Charlesworth et al., 2015). The index N75K mutation in *HPCA* alters a neutral asparagine residue in the second EF hand to a positively charged lysine, likely interfering with calcium binding in a loss-of-function manner.

Hippocalcin undertakes pleiotropic roles in mammalian neurons (Braunewell and Klein-Szanto, 2009), including acting as a calcium sensor to gate the slow afterhyperpolarisation (sAHP), a calcium-dependent potassium current, and facilitating NMDA receptor endocytosis during LTD (Jo et al., 2010; Tzingounis et

al., 2007). In *Drosophila*, NCA has previously been shown to be broadly expressed throughout the adult nervous system (Teng et al., 1994), yet the neuronal and organismal roles of NCA are unknown. Here we show that NCA is required to promote sleep by suppressing locomotor activity during the night. We demonstrate that NCA acts in a common pathway with the D1-type Dop1R1 dopamine receptor and identify a multi-component wake-promoting neuronal network in which NCA facilitates sleep by suppressing synaptic release. Thus, we propose that Hippocalcin homologs play conserved roles in regulating aspects of motor control.

Results

Generation of *Nca* knockout flies

The *Drosophila* genome contains a single *HPCA* homolog, *Neurocalcin* (*Nca*). Hippocalcin and NCA share > 90% amino-acid identity (Figure 1 – figure supplement 1A), suggesting conservation of function. To investigate the neuronal and behavioral roles of NCA we generated a *Nca* null allele by replacing the entire *Nca* locus (including 5' and 3' UTRs) with a mini-*white*$^{+}$ marker sequence using ends-out homologous recombination (Baena-Lopez et al., 2013) (Figure 1A, Figure 1 – figure supplement 1B-C). The mini-*white*$^{+}$ sequence is flanked by loxP sites, allowing removal by Cre recombinase and leaving single attP and loxP sites in place of the *Nca* locus (Figure 1A). As expected, no *Nca* mRNA expression was detected in homozygotes for the deleted *Nca* locus (Figure 1 – figure supplement 1D, E). Thus, we term this allele *Nca*^{KO} (*Nca* knockout).

Nca knockout flies exhibit reduced night sleep

Following outcrossing into an isogenic *iso31* control background, *Nca*^{KO} homozygotes were viable to the adult stage, allowing us to test whether NCA impacts locomotor control. To do so, we first used a high-throughout yet low resolution system, the *Drosophila* Activity Monitor (DAM) (Pfeiffenberger et al., 2010a), which counts locomotor activity via perturbations of an infrared beam intersecting a glass tube housing individual flies. Using this system, under 12 h light: 12 h dark conditions (12L: 12D, 25°C) we found that *Nca*^{KO} males exhibited two distinct locomotor phenotypes. Firstly, reduced maximal locomotor activity in response to lights-off (also termed the startle response or masking) (Figure 1 – figure supplement 2A, B). Secondly, increased locomotor activity during the night but not the day

107 (Figure 1 – figure supplement 2A, C, D). This later phenotype was suggestive of
108 reduced night sleep. We therefore quantified sleep levels in *Nca*^{KO} males and controls
109 using a 5 min period of inactivity to define a sleep bout – the standard definition in
110 the field (Pfeiffenberger et al., 2010b). Indeed, *Nca*^{KO} males exhibited reduced night
111 sleep but not day sleep relative to controls (Figure 1 – figure supplement 3).
112 Interestingly, the impact of removing NCA on night sleep appeared further enhanced
113 by shortening photoperiod, such that night (but not day) sleep was substantially
114 reduced in *Nca*^{KO} males under 8L: 16D (Figure 1B-D). Similarly to 12L: 12D, peak
115 locomotor activity following lights-off was reduced in *Nca*^{KO} males under 8L: 16D,
116 and the number of beam breaks during the normally quiescent period of the night was
117 increased (Figure 1 – figure supplement 4).
118 To obtain a higher resolution analysis of locomotor patterns in *Nca*^{KO} flies we
119 next utilized a video-tracking method - the DART (*Drosophila* ARousal Tracking)
120 system (Faville et al., 2015). Continual video-monitoring of *Nca*^{KO} males and *iso31*
121 controls confirmed robust sleep loss in *Nca*^{KO} males specifically during the night
122 (Figure 1E-G) accompanied by significantly shortened sleep bouts (Figure 1 – figure
123 supplement 5). By examining locomotor patterns in individual flies, we found that
124 *Nca*^{KO} males consistently displayed prolonged activity relative to controls following
125 lights-off and frequent bouts of movement even in the middle of the night, a period of
126 quiescence in *iso31* controls (Figure 1H, I). The velocity of locomotion in *Nca*^{KO}
127 males was also significantly increased relative to moving controls in the normally
128 quiescent period of the night (4-12 h after lights-off), whereas peak velocity during
129 the startle response to lights-off was reduced (Figure 1 – figure supplement 6), in
130 agreement with data collected using the DAM system. Collectively, the above data

131 suggest that complete loss of NCA results in both locomotor deficits and profound
132 nighttime hyperactivity, resulting in reduced peak levels of activity and night sleep.
133
134 **NCA is required in neurons to promote night sleep**
135 To identify the cellular substrates in which NCA acts to regulate locomotion and sleep
136 we performed cell-specific knockdown of *Nca* expression using transgenic RNA
137 interference (RNAi). NCA has been shown to be widely expressed in neuropil regions
138 throughout the *Drosophila* brain (Teng et al., 1994). Thus, we initially examined
139 neurons as a potential cellular candidate. We used three independent RNAi lines
140 (*kk108825, hmj21533* and *jf03398,* termed *kk*, *hmj* and *jf* respectively) to reduce *Nca*
141 expression in adult male neurons using the pan-neuronal *elav*-Gal4 driver. The *kk* and
142 *jf* dsRNAs target a partially overlapping sequence of *Nca*, whereas *hmj* targets a
143 distinct, non-overlapping upstream sequence (Figure 2 – figure supplement 1A). For
144 each RNAi line, we confirmed reduced *Nca* expression using qPCR (Figure 2 – figure
145 supplement 1B). Transcription of *Nca* occurs from promoter regions shared with the
146 downstream locus *cg7646*, yet *cg7646* transcription was not affected by *Nca* RNAi
147 (Figure 2 – figure supplement 1C), nor were any common off-target mRNAs
148 predicted for the *kk*, *hmj* or *jf* dsRNA hairpins (data not shown). Importantly, under
149 8L: 16D conditions, pan-neuronal expression of all three *Nca* RNAi lines specifically
150 reduced night sleep in males as measured by the DAM system (Figure 2A-C, Figure 2
151 – figure supplement 2). However, *Nca* knockdown did not result in a reduction in
152 peak locomotor activity as observed in Nca^{KO} males (Figure 2 – figure supplement 3).
153 Thus, neuronal NCA predominantly impacts sleep/activity during the night, with
154 NCA potentially acting in other cell types to regulate peak locomotor levels. We

155 therefore focused on elucidating the genetic pathways and neuronal circuits in which
156 NCA acts to promote night sleep.
157 To test whether sleep loss caused by neuronal *Nca* knockdown flies was due to
158 an indirect effect on the circadian clock, we examined whether *Nca* knockdown
159 altered circadian patterns of locomotor activity under constant dark conditions (Figure
160 2 – figure supplement 4A, B). Importantly, knockdown of *Nca* in neurons did not alter
161 circadian rhythmicity (Figure 2 – figure supplement 4A, B), nor did *Nca* expression
162 cycle in whole fly heads (Figure 2 – figure supplement C). Thus, it is unlikely that
163 sleep loss caused by neuronal *Nca* knockdown is due to circadian clock dysfunction.
164 We extended our initial findings in *Nca* knockdown males harbouring the pan-
165 neuronal *elav*-Gal4 driver and found that night sleep loss due to neuronal *Nca*
166 knockdown was also observed in adult virgin females (Figure 2 – figure supplement
167 5), and in male flies expressing the *kk Nca* RNAi using distinct pan-neuronal (*nsyb*-
168 Gal4) or broadly expressed (*insomniac*-Gal4) drivers (Figure 3A). In contrast,
169 expression of the *kk Nca* RNAi in muscle cells did not alter night sleep in adult males
170 (Figure 2 – figure supplement 6), supporting the premise that NCA acts in the nervous
171 system to regulate sleep. Video tracking further confirmed that neuronal expression of
172 *kk Nca* RNAi reduced night sleep (Figure 2D-F). Collectively, the above data
173 demonstrate that NCA acts in neurons to promote night sleep in *Drosophila*. For
174 simplicity, we use the *kk Nca* RNAi for all subsequent experiments, and refer to flies
175 expressing *kk Nca* RNAi under *elav*-Gal4 as Nca^{KD} (*Nca* knockdown). Given the
176 similar results obtained using the DAM and DART systems for both Nca^{KO} and
177 Nca^{KD} flies, we use DAM as a high-throughput method for all sleep measurements
178 detailed below, which are performed in 8L: 16D conditions at 25°C.
179

180 **NCA acts in a common pathway with the Dop1R1 dopamine receptor**

181 In *Drosophila*, dopamine is a pro-arousal factor, with elevated dopaminergic
182 neurotransmission strongly reducing sleep (Kume et al., 2005). Recent studies have
183 shown that the pro-arousal effect of elevated dopamine is mediated by the D1-type
184 Dop1R1 dopamine receptor (Liu et al., 2012; Ueno et al., 2012). Furthermore, both
185 hypo- and hyper-dopaminergic signalling within the human basal ganglia has been
186 proposed to underlie forms of primary dystonia (Breakefield et al., 2008). We
187 therefore tested whether *Nca* promotes sleep in a common pathway with genes
188 involved in dopaminergic signalling. Indeed, we found that heterozygosity for a null
189 or strongly hypomorphic allele of the *Dop1R1* dopamine receptor (*Dop1R1*$^{\text{MI03085-}}$
190 $^{\text{GFST.2}}$, a homozygous lethal MiMIC insertion) rescued night sleep loss in *Nca*^{KD} flies
191 (Figure 2G, H). Importantly, in both *elav*-Gal4/+ and *kk*/+ control backgrounds,
192 heterozygosity for *Dop1R1*$^{\text{MI03085-GFST.2}}$ did not alter sleep levels (Figure 2G, H; $p >$
193 0.05, Kruskal-Wallis test with Dunn's post-hoc test). A similar epistatic interaction
194 between *Nca* and *Dop1R1* was observed using a second, weaker *Dop1R1* allele
195 (*Dop1R1*$^{\text{MI004437}}$) (Figure 2 – figure supplement 7).

196 Mammalian Hippocalcin regulates cell-surface levels of NMDA receptors
197 during LTD (Jo et al., 2010), and *Drosophila nmda receptor 1* (*dNR1*) mutants exhibit
198 reduced sleep during the night (Tomita et al., 2015), similarly to *Nca* knockout and
199 knockdown flies. However, in contrast to *Dop1R1*, we found no signatures of genetic
200 interaction between *Nca* and *dNR1*, suggesting that these loci act in distinct pathways
201 to promote sleep (Figure 2 – figure supplement 8).

202

203 **NCA acts in two distinct circuits to promote night sleep**

204 We next sought to delineate the neural circuits in which NCA functions to promote
205 night sleep. Using transgenic RNAi, we performed an extensive screen of sleep
206 relevant circuits defined by numerous *promoter*-Gal4 driver lines (Figure 3A, Figure
207 3 – figure supplement 1). These include clock neurons, dopaminergic and other
208 neurotransmitter-specific subtypes, fan-shaped body neurons, mushroom body (MB),
209 and sensory neurons (Figure 3A) (Donlea et al., 2011; Joiner et al., 2006; Lamaze et
210 al., 2017; Liu et al., 2014; Pitman et al., 2006; Seidner et al., 2015; Sitaraman et al.,
211 2015). Given the genetic interaction between *Nca* and *Dop1R1*, we also utilised
212 genomic enhancer elements in the *Dop1R1* locus to drive *Nca* knockdown in subsets
213 of potential Dop1R1-expressing neurons (Figure 3A, Figure 3 – figure supplement 1)
214 (Jenett et al., 2012; Jiang et al., 2016). However, in contrast to broadly expressed
215 drivers (*elav*-, *nsyb*- and *inc*-Gal4), *Nca* knockdown in restricted neural subsets was
216 insufficient to significantly reduce night sleep (Figure 3A, Figure 3 – figure
217 supplement 1).
218 These results suggested a complex sleep-relevant circuit requirement for
219 NCA. We therefore reduced NCA levels in multiple sub-circuits to test for a
220 simultaneous role of NCA in distinct anatomical regions. Through this approach, we
221 found that *Nca* knockdown using two *enhancer*-Gal4 lines (*R14A05* – an enhancer in
222 the *single-minded* locus, and *R72C01* – an enhancer in the *Dop1R1* locus; see Figure
223 3B for expression patterns) was sufficient to strongly phenocopy the effect of pan-
224 neuronal *Nca* knockdown on night sleep (Figure 3C, D; compare Figure 3C with
225 Figure 2A). For simplicity we refer to these drivers as *A05* and *C01* respectively.
226 The *A05* enhancer drives expression in approximately 70 neurons, as
227 quantified using a fluorescent nuclear marker (Figure 3 – figure supplement 2A, B)
228 that include a subset of MB neurons, a cluster of cell bodies adjacent to the anterior

229 ventrolateral protocerebrum (AVP), and two visual sub-circuits: optic lobe (OL) and
230 anterior optic tubercle (AOTU) neurons (Figure 3B). *C01* drives expression in
231 approximately 250 neurons (Figure 3 – figure supplement 2C, D) that include the
232 MBs, neurons projecting to the MB γ-lobes, the antennal mechanosensory and motor
233 center (AMMC) (Figure 3B) and the superior medial protocerebrum (SMP). Both
234 drivers label additional cell bodies of unknown identity. The potential overlap of *A05*
235 and *C01* in the MBs raised the possibility that sleep loss in *A05/C01 > Nca* RNAi
236 flies was due to strong NCA knockdown in neurons common to both the *A05* and *C01*
237 enhancers. If so, driving *Nca* RNAi with two copies of either *A05* or *C01* should
238 mimic sleep loss in *A05/C01 > Nca* RNAi flies. However, this was not the case
239 (Figure 4 – figure supplement 3). Thus, NCA is simultaneously required in two non-
240 overlapping sub-circuits defined by the *A05* and *C01* enhancers.
241 Given that *C01* is a *Dop1R1* enhancer element, that *Nca* and *Dop1R1*
242 genetically interact to regulate sleep (Figure 2G, H), and that Dop1R1 is highly
243 expressed in the MBs (Lebestky et al., 2009), we tested whether the MBs were a
244 constituent of the *C01* expression domain by swapping *C01* for the MB-specific
245 driver *ok107* and measuring sleep in flies expressing *Nca* RNAi in both *A05* and MB
246 neurons. Indeed, knockdown of *Nca* in both *A05* and MB neurons also specifically
247 reduced night sleep (Figure 3 – figure supplement 4), albeit to a weaker degree
248 compared to knockdown in *A05* and *C01* neurons (compare with Figure 3C, D). Thus,
249 we conclude that the MBs are a component of a complex network defined by *C01*-
250 Gal4 with additional, as yet undefined, neurons acting within both the *C01* and *A05*
251 domains to regulate night sleep.
252

253 **NCA promotes sleep by suppressing synaptic output from a wake-promoting**
254 **circuit**

255 We next assessed how NCA impacts excitability of *C01* and *A05* neurons. To do so,
256 we expressed a genetically-encoded fluorescent indicator of neurotransmitter release,
257 UAS-*synaptopHluorin* (*spH*) (Miesenbock, 2012), in *C01* and *A05* neurons of either
258 wild type or Nca^{KD} males. spH is localised to presynaptic neurotransmitter-containing
259 vesicles and increases in fluorescence in a pH-dependent manner upon fusion of
260 synaptic vesicles with the presynaptic membrane, providing an optical read-out of
261 neurotransmitter release (Miesenbock, 2012). Intriguingly, we found that *Nca*
262 knockdown significantly enhanced spH fluorescence in the MB α/β-lobes and the
263 AMMC but not in the MB γ-lobe region or the SMP (Figure 4).

264 Since neurotransmitter release is enhanced in subsets of *C01* and *A05* neurons
265 following *Nca* knockdown, this suggested that NCA normally acts to inhibit synaptic
266 output in these circuits. If sleep loss in *Nca* knockdown flies directly results from a
267 loss of such inhibition in *C01* and *A05* neurons (thus enhancing neurotransmitter
268 release), we predicted the following: firstly, that artificial activation of *C01* and *A05*
269 neurons should be sufficient to promote locomotor activity (and thus sleep loss), and
270 secondly, that silencing *C01* and *A05* neurons should suppress sleep loss in *Nca*
271 knockdown flies. To test our first prediction, we enhanced the excitability of *C01* and
272 *A05* neurons by expressing the temperature-sensitive channel TrpA1 in either
273 neuronal subset or both and shifting flies from a non-activating temperature (22°C) to
274 an activating temperature (27°C) sufficient to cause neural excitation through TrpA1-
275 mediated cation influx (Hamada et al., 2008) (Figure 5A). At the non-activating
276 temperature, over-expression of TrpA1 in either circuit or both did not alter sleep
277 levels (Figure 5B). At the activating temperature, excitation of *A05* neurons did not

278 alter night sleep levels relative to controls (Figure 5C, D). In contrast, excitation of
279 *C01* neurons profoundly reduced night sleep (Figure 5C, D) as well as day sleep
280 (Figure 5C). Interestingly, simultaneous activation of *C01* and *A05* neurons further
281 reduced night sleep but not day sleep relative to activation of *C01* neurons alone
282 despite the lack of effect of *A05* neuron activation on sleep (Figure 5C, D).
283 To test our second prediction, we over-expressed a non-inactivating outward
284 rectifying potassium channel (dORKΔC2) in *C01* and *A05* neurons with and without
285 *Nca* knockdown via RNAi. Here, expression of dORKΔC2 is predicted to suppress
286 neuronal firing by hyperpolarizing the resting membrane potential (Nitabach et al.,
287 2002; Park and Griffith, 2006). Silencing *C01* and *A05* neurons with dORKΔC2 in an
288 otherwise wild type background did not alter day or night sleep levels (Figure 5E, F).
289 However, consistent with our above prediction, dORKΔC2 expression significantly
290 suppressed night sleep loss due to *Nca* knockdown in *C01* and *A05* neurons (Figure
291 5E, F). Thus, we propose that NCA promotes night sleep by limiting synaptic output
292 from a multi-component activity-promoting circuit coordinately defined by subsets of
293 the *C01*- and *A05*-Gal4 expression domains. Our results further suggest that the *C01*
294 and *A05* circuits interact to suppress sleep, with *C01* neurons acting as a predominant
295 pro-arousal circuit and *A05* neurons acting in a modulatory manner to enhance the
296 impact of *C01* activation on night sleep.
297
298
299

300 **Discussion**

301 Previous work has demonstrated that *Drosophila* Neurocalcin (NCA), a member of
302 the neuronal calcium sensor family, is widely expressed throughout the fly brain and
303 localizes to synaptic regions (Teng et al., 1994). However, the neurobiological
304 functions of NCA have remained unclear. Here we define a role for NCA in
305 promoting night sleep and show that NCA acts via inhibiting synaptic output from a
306 complex movement-promoting circuit.

307 Previous genetic screens have identified an array of sleep-promoting factors in
308 *Drosophila* (Tomita et al., 2017). However, despite extensive circuit analyses, the
309 activity of such proteins does not fully map onto known sleep-regulatory neurons, and
310 the complete neural substrates in which these factors act have yet to be determined
311 (Afonso et al., 2015; Rogulja and Young, 2012; Shi et al., 2014; Stavropoulos and
312 Young, 2011; Tomita et al., 2015; Wu et al., 2014). Our results are consistent with
313 these findings and offer a tentative explanation for the difficulties in defining circuit
314 requirements for sleep-relevant proteins. We show that NCA activity is not required
315 within a single cell-type or neuropil region to promote sleep. Instead, sleep-relevant
316 NCA activity can largely be localised to *two* distinct domains of the *Drosophila*
317 nervous system defined by the *A05*- and *C01*-Gal4 drivers. One relevant cell-type
318 within these domains is the mushroom bodies (MBs), a known sleep-regulatory center
319 (Joiner et al., 2006; Pitman et al., 2006; Sitaraman et al., 2015). However, the MBs
320 only partially contribute to one of the two sleep-relevant domains, indicating that
321 NCA acts in a dispersed network that likely incorporates several non-overlapping
322 wake-promoting circuits.

323 Interestingly, whereas activation of *C01* neurons is sufficient to suppress
324 sleep, activation of *A05* neurons reduces night but not day sleep only in the context of

325 *C01* neuron activation. We note that activation of *C01* neurons profoundly reduces
326 sleep during both day and night periods, whereas only night sleep is impaired in flies
327 with reduced NCA expression in *C01* and *A05* neurons. Based on these findings, we
328 hypothesize that reduction of NCA in *C01* and *A05* neurons causes mild
329 hyperexcitation, which in *C01* neurons alone is insufficient to modulate sleep but in
330 both *C01* and *A05* neurons simultaneously causes an increase in network excitability
331 sufficient to reduce night sleep. A selective inhibition of neurotransmitter release by
332 NCA in subsets of *C01* and *A05* neurons is supported by our in vivo imaging data
333 showing that *Nca* knockdown increases synaptic output in the MB α/β-lobes and
334 AMMC but not the MB γ-lobe region or the SMP. Since NCA is only partly required
335 in the MBs, we consider it unlikely that increased synaptic output within the MBs and
336 AMMC alone is sufficient to drive sleep loss in *Nca* knockdown flies. Rather, we
337 propose that coincident hyperactivity of several sub-circuits within the *C01* and *A05*
338 domains collectively drives night sleep loss. Temporal information encoded by light-
339 sensing or circadian pathways may further demarcate the period in which NCA
340 promotes sleep (i.e the night), with such inputs likely to be bypassed by ectopic
341 activation of *C01* neurons, resulting in sleep loss across 24 h.
342 Since silencing of *C01* and *A05* neurons does not alter basal sleep, we suggest
343 that these circuits are normally activated by an ethological stimulus absent during our
344 experimental conditions. We further postulate that modulatory dopamine signalling
345 through Dop1R1 promotes neural activity in wake-promoting *C01* neurons. These
346 neurons are defined by a *Dop1R1* enhancer element, and thus it is likely that at least a
347 subset of *C01* neurons express Dop1R1. Indeed, dopamine signalling via Dop1R1 has
348 been shown to enhance synaptic transmission between antennal lobe projection
349 neurons and MB neurons (Ueno et al., 2013). This model is attractive since reducing

350 such input could balance the increased synaptic release caused by *Nca* knockdown,
351 providing an explanatory basis for the genetic interaction between *Nca* and *Dop1R1*.
352 How might NCA inhibit synaptic output from *C01* and *A05* neurons? The
353 mammalian NCA homolog Hippocalcin acts pleiotropically in several pathways that
354 control neuronal excitability and plasticity, facilitating NMDA receptor endocytosis
355 during LTD and gating the slow afterhyperpolarisation, a calcium-activated potassium
356 current controlling spike frequency adaptation that is thought to be mediated by a
357 complex array of potassium channels (Andrade et al., 2012; Jo et al., 2010;
358 Tzingounis et al., 2007). Recent data suggest that Hippocalcin also negatively
359 regulates calcium influx through N-type voltage-gated calcium channels (Helassa et
360 al., 2017). Given the strong homology between Hippocalcin and NCA, it is possible
361 that NCA suppresses neurotransmitter release through similar pathways in *Drosophila*
362 neurons, although the lack of genetic interaction between *Nca* and the *dNR1* NMDA
363 receptor suggests that an enhancement of NMDA receptor levels is unlikely to
364 significantly contribute to sleep loss in *Nca* knockout/knockdown flies.
365 Mutations in Hippocalcin also cause the movement disorder DYT2 primary
366 isolated dystonia (Charlesworth et al., 2015). What is the common neurobiological
367 link between dystonic movements in humans and sleep loss in *Drosophila*? We
368 suggest that both phenotypes fundamentally reflect a dysregulation of motor control
369 i.e when activity is initiated, and for how long such activity is maintained.
370 Hippocalcin/Neurocalcin homologs have the potential to act as molecular toggle
371 switches, inhibiting sustained rapid-firing and neurotransmitter release in activity-
372 promoting neurons via simultaneous modulation of potassium and calcium channel
373 function (Helassa et al., 2017; Tzingounis et al., 2007). Mutations in these calcium
374 sensors may thus result in prolonged bouts of synaptic output and corresponding

375 motor activity. We note that *insomniac*, another sleep-promoting gene in *Drosophila*,
376 is homologous to the myoclonus dystonia-gene *KCTD17* (as well the paralogs *KCTD2*
377 and *KCTD5*) (Li et al., 2017; Mencacci et al., 2015; Stavropoulos and Young, 2011).
378 It will thus be intriguing to test if other dystonia gene homologs also promote sleep in
379 *Drosophila,* and whether human dystonia and *Drosophila* sleep loss can thus be
380 considered homologous phenotypes (or phenologs) linked to mutations in a conserved
381 genetic network that functions to suppress inappropriate activity in both humans and
382 flies (Lehner, 2013; McGary et al., 2010).
383

384 **Materials and Methods**

385 **Fly husbandry**

386 Flies were maintained on standard fly food at constant temperature 25°C under 12 h:
387 12 h light-dark cycles (12L: 12D). The following strains were obtained from the
388 Bloomington and VDRC stock centers: kk108825 (v100625), hmj21533 (54814),
389 jf03398 (29461), *Dop1R1*$^{\text{MI03085-GFSTF.2}}$ (59802), *Dop1R1*$^{\text{MI04437}}$(43773), *ple*-Gal4
390 (8848), *Chat*-Gal4 (6798), *vGlut*-Gal4 (26160), *GAD*-Gal4 (51630), *Ddc*-Gal4(7010),
391 *GMR*-Gal4 (1104), *Trh.1*-Gal4 (38388), *Tdc2*-Gal4(9313), *C5*-Gal4 (30839), *ok107*-
392 Gal4 (854) and *A502* (16130). The remaining lines obtained from the Bloomington
393 stock center are part of the Janelia Flylight collection with identifiable prefixes:
394 R23E10-Gal4, R55B01-Gal4, R52H12-Gal4, Hdc-Gal4 (R17F12-Gal4), R14A05-
395 Gal4, R72B05-Gal4, R72B07-Gal4, R72B08-Gal4, R72B11-Gal4, R72C01-Gal4, and
396 R72C02-Gal4. The following lines were gifts from laboratories of Kyunghee Koh:
397 *elav*-Gal4, *nsyb*-Gal4, *tim*-Gal4 and *TUG*-Gal4; Joerg Albert: *nompC*-Gal4
398 (Kamikouchi et al., 2009) and Nicolas Stavropouplos: *inc*-Gal4:2 (Stavropoulos and
399 Young, 2011). *ppk*-Gal4 and *TrpA1*-CD-Gal4 were described previously (Zhong et
400 al., 2012). *GMR-hid*, *tim*^{KO} and *cry*^{02} were previously described in (Lamaze et al.,
401 2017). Except for *Ddc*-Gal4, *Trh.1*-Gal4, *Tdc2*-Gal4, *nompC*-Gal4 and *Hdc*-Gal4, all
402 *Drosophila* strains above were either outcrossed five times into an isogenic control
403 background (*iso31*) or insertion-free chromosomes were exchanged with the *iso31*
404 line (*hmj21533, jf03398, Dop1R1*$^{MI03085-G}$, *Dop1R1*^{MI04437} and *NMDAR1*$^{\text{MI11796}}$) before
405 testing for sleep-wake activity behaviour. Note: R14A05-Gal4 was initially
406 mislabelled as R21G01-Gal4 in Bloomington shipment. The clear mismatch between
407 the image of R21G01>GFP in FlyLight database and our immunostaining data (A05,
408 Fig3B) led us to clarify the identity of the line, as R14A05-Gal4, by sequencing

409 genomic PCR product using primers pair: pBPGw_ampF: agggttattgtctcatgagcgg and
410 pBPGw_Gal4R: ggcgcacttcggtttttctt.

411 **Generation of the *Nca^{KO}* line**

412 Null alleles of *Nca* were generated using homologous recombination as described
413 previously (Baena-Lopez et al., 2013). Briefly, genomic DNA was extracted from 20
414 wild type flies (Canton S) using the BDGP buffer A-LiCl/KAc precipitation protocol
415 (http://www.fruitfly.org/about/methods/inverse.pcr.html). The 5' (Arm 1) and 3'
416 (Arm 2) genomic regions flanking the *Nca* coding sequence were PCR amplified via
417 high fidelity DNA polymerase (Q5 high-fidelity 2X master mix, M0492S, NEB) with
418 the following primers: NotI_Arm1F1:gcggccgctaatttgcagctctgcatcg,
419 NotI_Arm1R1:gcggccgcatggtaagaagcacgcaacc,
420 AscI_Arm2F1:ggcgcgccttatgaccgttccaaaacacc,
421 AvrII_Arm2R1:cctaggggctaaatacgttgaccaagc. The corresponding Arm1 and Arm2
422 fragments (~2.5kb) were gel purified (Wizard® SV Gel and PCR Clean-Up System,
423 A9281, Promega) and cloned into pCR-Blunt II-TOPO vector (Zero Blunt® TOPO®
424 PCR Cloning Kit, 450245, ThermoFisher Scientific), and subsequently sub-cloned via
425 NotI (R3189S, NEB) and AscI/AvrII digestion (R0558S and R0174S, NEB) and T4
426 ligation (M0202S, NEB) into pTV vector, a P-element construct containing the mini-
427 *white*$^{+}$ marker and UAS-*reaper* flanked by FRT and I-SceI sites (Baena-Lopez et al.,
428 2013). The sequence identifies of Arm 1 and Arm 2 fragments within the pTV vector
429 were verified via Sanger sequencing using the following primers: nca1_f:
430 cagctctgcatcgctttttgt, nca1_3_f: ccctcgcgcatggtacttta, nca1_r: agcgtcacataagttctccca,
431 nca1_4_f: tggacgaaaataacgatggtca, nca1_5_f: agactacttagccatgttttcatact, nca1_2_f:
432 tgacgaagccacaattaaagagtg, nca1_1_f: gcaaccctgttccccttttca,

433 nca2_f: gaccgttccaaaacaccca, nca2_3_f: ttgttgtgcgccacgttttc, nca2_r:
434 acgtatgctccatgattcctct
435 nca2_4_f: tgcaggtcggttaatcaatgc, nca2_5_f: tcaatcgatttggggccagg, nca2_2_f:
436 ccttctccaggctcagcaaa, nca2_1_f: actctgcatttcgataagattagcc. Donor lines containing
437 pTV vector with Arm1 and Arm2 homologous fragments (pTV_nca1+2) were then
438 generated via embryonic injection and random P-element mediated genomic
439 insertions (Bestgene, inc.). To initiate homologous recombination between
440 pTV_nca1+2 and the endogenous *Nca* locus, donor lines were crossed to *yw*; hs-*flp*,
441 hs-I-*SceI*/CyO and the resulting larvae were heat shocked at 48 h and 72 h after egg
442 laying for 1 h at 37°C. Around 200 female offspring with mottled/mosaic red eyes
443 were crossed in pools of three to *ubiquitin*-Gal4[3xP3-GFP] males to remove
444 nonspecific recombination events (via UAS-*reaper*-mediated apoptotic activity). The
445 crossings were flipped once over and the progeny (~12000 adults) was screened for
446 the presence of red-eyed and GFP-positive flies. Three independent GFP^+ red-eyed
447 lines (*ko1*, *ko2*, and *ko3*) were identified. The exchange of endogenous *Nca* locus with
448 pTV_nca1+2 fragments was confirmed by detecting a 2.6 kb PCR product (Figure 1
449 figure supplement 1C) in the genomic DNA samples of the above three lines (pre-
450 digested by EcoRI/NotI) using the following primer pairs: ncaKO-F2:
451 tgggaattgactgatacagcct; ncaKO-R2: ggcactacggtacctgcat. ncaKO-F2 matches to the
452 region between 24 bp and 2 bp upstream of Arm1 and ncaKO-R2 overlaps with attP
453 site (Figure 1A). The absence of endogenous *Nca* mRNA in *ko1* flies was confirmed
454 by standard and quantitative RT-PCR (Figure 1 figure supplement 1D; see also the
455 below RNA section). The min-$white^+$ cassette and majority of pTV vector sequences
456 were further removed from the *ko1* genome via Cre-loxP recombination (Figure 1A).
457 This "Cre-out" strain was then backcrossed five times to a Nca^{A502} line (where *A502*

458 is a P-element insertion 2 kbp upstream of the *Nca* CDS) that was outcrossed
459 previously into the *iso31* background (see Fly husbandry section). Before testing for
460 changes in sleep/wake behaviour, the resulted line, termed *Nca* knockout (Nca^{KO}),
461 was lastly verified by sequencing a 576 bp genomic PCR product (using primer pair:
462 nca1_5_f and nca2_r), confirming the absence of *Nca* CDS sequence and the insertion
463 an attP site in the *Nca* locus.

464 **RNA extraction and Quantitative PCR**

465 For RNA extractions, 10-20 fly heads per genotype were collected with liquid
466 nitrogen and dry ice. Total RNA was extracted using TRIzol™ reagent following
467 manufacturer's manual (Thermo Fisher Scientific). cDNA was reverse transcribed
468 from 250 or 500 ng of DNase I (M0303S, NEB) treated RNA via MMLV RT
469 (M170A, Promega). A set of five or six standards across 3125-fold dilution was
470 prepared from the equally pooled cDNA of all genotypes in each experiment.
471 Triplicated PCR reactions were prepared in 96-well or 384-well plates for standards
472 and the cDNA sample of each genotype (20 to 40 fold dilution) by mixing in Power
473 SYBR Green Master Mix (Thermo Fisher Scientific) and the following primer sets:
474 ncaqF2: acagagttcacagacgctgag, ncaqR2: ttgctagcgtcaccatatggg; cg7646F:
475 gcctttcgaatgtacgatgtcg, cg7646R: cctagcatgtcataaattgcctgaac or
476 rp49F:cgatatgctaagctgtcgcaca, rp49R: cgcttgttcgatccgtaacc. PCR reactions were
477 performed in Applied Biosystems StepOne (96-wells module) or QuantStudio 6Flex
478 instruments (384 wells module) using standard thermocycle protocols. Melting curve
479 analysis was also performed to evaluate the quality of the PCR product and avoid
480 contamination. The Ct values were exported as csv files and a standard curve between
481 Ct values and logarithm of dilution was calculated using the liner regression function
482 in Graphpad. The relative expression level for *Nca*, *cg7646* and *rp49* of each sample

483 were estimated by interpolation and anti-logarithm. The expression levels of *Nca* and
484 *cg7646* for each genotype were further normalized to their respective average *rp49*
485 expression level. Statistical differences between the normalized expressions levels of
486 each genotype were determined by Mann-Whitney test or Kruskal-Wallis test with
487 Dunn's post-hoc test using Graphpad software.

488 **Sleep-wake behavioral analysis**

489 Three to five days old male or virgin female flies were collected and loaded into glass
490 tubes containing 4% sucrose and 2% agar (w/v). Sleep-wake behavior was recorded
491 using the *Drosophila* Activity Monitor (DAM, TriKinetics, inc.) system or
492 *Drosophila* ARousal Tracking (DART, BFKlab) system for 3 days in the designated
493 LD regime (L12: D12 or L8: D16) at 25°C. Behavioral recordings from the third day
494 of the given LD regime were then analyzed. All flies were entrained to 12L: 12D
495 prior to entering designated LD regimes. For ectopic activation experiments involving
496 UAS-*TrpA1*, flies were cultured in 18°C during development and then entrained to
497 L8: D16 at 22°C before entering L8: D16 condition at 27°C. *Drosophila* activity (or
498 wake) is measured by infra-red beam crosses in DAM or by direct movement tracking
499 in DART. Sleep is defined by 5 minutes of inactivity (where inactivity is defined as
500 no beam crosses during 1 min in the DAM or less than 3 mm movement in 5 s in
501 DART). The csv output files with beam crosses (DAM) or velocity data (DART)
502 were processed by a customized Excel calculators (Supplementary file 1) and R-
503 scripts (https://github.com/PatrickKratsch/DAM_analysR) to calculate the following
504 parameters for individual flies: *Onset and offset of each sleep bout*, *sleep bout length*,
505 *day and night sleep minutes*, *daily total sleep minutes,* and *daily sleep profile* (30
506 minutes interval). An established MATLAB® based tool, Flytoolbox, was used for
507 circadian rhythmicity analysis (Levine et al., 2002a, b). Briefly, the strength of

508 rhythmicity (RI) was estimated using the height of the third peak coefficient in the
509 auto-correlogram calculated for the activity time series of each fly. Rhythmic
510 Statistics values were then obtained from the ratio of the RI value to the 95%
511 confidence interval for the correlogram ($2/\sqrt{N}$, where N is the number of
512 observations, which correlatively increase with the sampling frequency), in order to
513 determine statistical significance of any identified period (RS is ≥ 1)

514 **Immunohistochemistry and confocal microscopy**

515 Adult male R72C01 > CD8::*GFP* and R21G01 > CD4::*tdTomato* flies were
516 anesthetized in 70% ethanol before brains were dissected in PBT (0.1M phosphate
517 buffer with 0.3% TritonX100) and collected in 4% paraformaldehyde/PBT on ice.
518 The fixation was then performed at room temperature for 15 min before washing 3
519 times with PBT. The brain samples were blocked using 5% goat serum/PBT for 1 h at
520 room temperature before incubation with primary antibodies. The samples were
521 washed 6 times with PBT before incubated with Alexa Fluor secondary antibodies in
522 5% goat serum/PBT at 4°C over 24 h. After washing 6 times with PBT, the samples
523 were mounted in SlowFade Gold antifade reagent (S36936, Thermo Fisher Scientific)
524 on microscope slides and stored at 4°C until imaged using an inverted confocal
525 microscope Zeiss LSM 710. Primary antibody concentrations were as follows: mouse
526 anti-nc82 (Developmental Studies Hybridoma Bank) - 1:200; rabbit anti-GFP
527 (Invitrogen) - 1:1000; rabbit anti-dsRED (Clontech) - 1:2000. Alexa Fluor
528 secondaries (Invitrogen) were used as follows: Alexa Fluor 647 goat anti-mouse IgG -
529 1:500, Alexa Fluor 488 goat anti-rabbit IgG - 1:2000, Alexa Fluor 555 goat anti-rabbit
530 IgG - 1:2000. For quantification of nuclei number in *C01 > red-stinger* and *A05 >*
531 *red-stinger* brains, unstained Red-Stinger fluorescence was captured via confocal
532 microscopy. DAPI (Sigma Aldrich) was used to counterstain nuclei (at a dilution of

533 1:5000). The number of Red-Stinger-positive nuclei in each brain was subsequently
534 quantified using the ImageJ 3D Objects Counter tool, with a variable threshold used
535 to incorporate all of the visible Red-Stinger-positive nuclei.

536 **Synapto-pHluorin imaging**

537 Synaptic activity of C01/A05 neurons was monitored in *ex vivo* fly brains using UAS-
538 super-eclipse-synaptopHluorin construct (UAS-*spH*) (Miesenbock, 2012). Adult male
539 *C01/A05* > UAS-*spH* or *C01/A05* > UAS-*spH, kk* flies were housed in normal
540 behaviour tubes (see behaviour analysis section) and entrained for 3 days in L8: D16
541 condition at 25°C. Individual flies of either genotype were carefully captured between
542 ZT9 and ZT11 and fly brains were immediately dissected in HL3 *Drosophila* saline
543 (70 mM NaCl, 5 mM KCl, 1.5 mM $CaCl_2$, 20 mM $MgCl_2$, 10 mM $NaHCO_3$, 5 mM
544 Trehalose, 115 mM Sucrose and 5 mM HEPES, pH 7.2) at room temperature. Fly
545 brains were transferred into 200 μl HL3 in a poly-lysine treated glass bottom dish (35
546 mm, 627860, Greiner Bio-One) before imaging using an inverted confocal Zeiss LSM
547 710 microscope (20x objective with maximum pinhole). Three to five image stacks
548 (16 bits) were taken within two minutes to minimise tissue degradation and to cover
549 the depth of all spH-positive anatomical regions. Z-projections of the image stacks of
550 each brain were generated by ImageJ software before the fluorescent intensity of the
551 indicated neuropil centres was quantified using free drawn ROIs. Background
552 fluorescence measured by the same ROIs from areas with no brain tissue was then
553 subtracted to obtain the final fluorescent value. Mean fluorescent values of the
554 indicated neuropil regions in each hemisphere were calculated and compared between
555 genotypes. The statistical difference was determined by Mann-Whitney U-test using
556 Graphpad software.

557 **Bioinformatics**

Conservation of amino acid residues between *Drosophila* Neurocalcin and human Hippocalcin was determined using ClustalW2 software for multiple sequence alignment. Amino-acid identity and similarity was visualised using BOXSHADE.

Acknowledgements

We thank Jack Humphrey for performing initial work on *Neurocalcin* knockdown flies, and Kyunghee Koh and Simon Lowe for helpful comments on the manuscript. This study was supported by the Wellcome Trust (Synaptopathies strategic award [104033]), and by the MRC [New Investigator Grant MR/P012256/1]. P.K is supported by a Wellcome Trust Neuroscience PhD studentship.

Competing interests

The authors have no financial or non-financial competing interests.

573 **Figures and Figure legends**

Figure 1

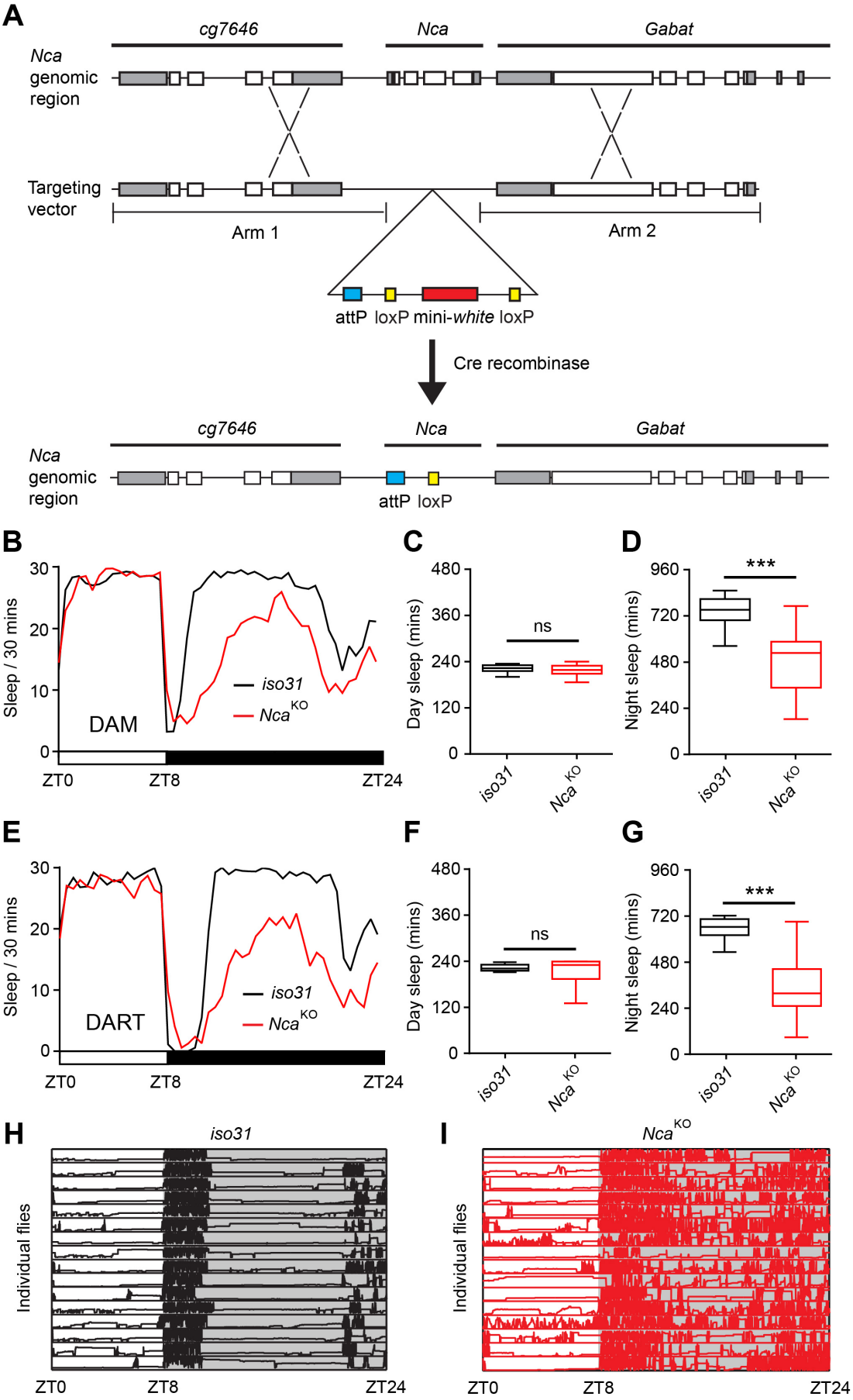
A
cg7646
Nca
Gabat
Nca genomic region
Targeting vector
Arm 1
Arm 2
attP loxP mini-white loxP
Cre recombinase
cg7646
Nca
Gabat
Nca genomic region
attP loxP
B
Sleep / 30 mins
DAM
iso31
Nca KO
ZT0
ZT8
ZT24
C
Day sleep (mins)
ns
iso31
Nca KO
D
Night sleep (mins)
***
iso31
Nca KO
E
Sleep / 30 mins
DART
iso31
Nca KO
ZT0
ZT8
ZT24
F
Day sleep (mins)
ns
iso31
Nca KO
G
Night sleep (mins)
***
iso31
Nca KO
H
iso31
Individual flies
ZT0
ZT8
ZT24
I
Nca KO
Individual flies
ZT0
ZT8
ZT24

574

575 **Figure 1.** *Neurocalcin* (*Nca*) knockout flies exhibit enhanced night activity and
576 reduced sleep. (A) Schematic illustration of the procedure used to generate a *Nca*
577 knockout allele. Homologous arms upstream (Arm 1) and downstream (Arm 2) of the
578 *Nca* locus are indicated. Following homologous recombination, the endogenous *Nca*
579 locus is replaced by a cassette containing the mini-*white* selection marker (red bar),
580 and attP (blue bar) and loxP sites (yellow bars). The mini-*white* cassette was
581 subsequently removed via Cre-loxP recombination. (B) Mean sleep levels in 8L: 16D
582 conditions for Nca^{KO} adult males and *iso31* controls measured using the *Drosophila*
583 Activity Monitor (DAM). (C-D) Median day (C) and night (D) sleep levels in the
584 above genotypes. (E) Mean sleep levels in 8L: 16D conditions for Nca^{KO} adult males
585 and *iso31* controls measured by the video-based *Drosophila* ARousal Tracking
586 system (DART). (F-G) Median day (F) and night (G) sleep levels in the above
587 genotypes. Data are presented as Tukey box plots. The 25th, Median, and 75th
588 percentiles are shown. Whiskers represent 1.5 x the interquartile range. Identical
589 representations are used in all subsequent box plots. B-D: n = 32 per genotype; E-G: n
590 = 16. (H-I) The longitudinal movement for individual *iso31* (H) and Nca^{KO} (I) flies
591 are shown as rows of traces plotting vertical position (Y-axis) over 24 h (X-axis)
592 under 8L: 16D condition. ***$p < 0.001$, ns - $p > 0.05$, Mann-Whitney U-test.
593
594

Figure 1 figure supplement 1

A

```
Hs HPCA    1  MGKQNSKLRPEMLQDLRENTEFSELELQEWYKGFLKDCPTGILNVDEFKKIYANFFPYGD
Dm NCA     1  MGKQNSKLKPEVLEDLKQNTEFTDAEIQEWYKGFLKDCPSGHLSVEEFKKIYGNFFPYGD

Hs HPCA   61  ASKFAEHVFRTFDTNSDGTIDFREFIIALSVTSRGRLEQKLMWAFSMYDLDGNGYISREE
Dm NCA    61  ASKFAEHVFRTFDANGDGTIDFREFLCALSVTSRGKLEQKLKWAFSMYDLDGNGYISRQE

Hs HPCA  121  MLEIVQAIYKMVSSVMKMPEDESTPEKRTEKIFRQMDTNNDGKLSLEEFIRGAKSDPSIV
Dm NCA   121  MLEIVTAIYKMVGSVMKMPEDESTPEKRTDKIFRQMDRNKDGKLSLEEFIEGAKSDPSIV

Hs HPCA  181  RLLQCDPSSASQF
Dm NCA   181  RLLQCDPQSH---
```

B

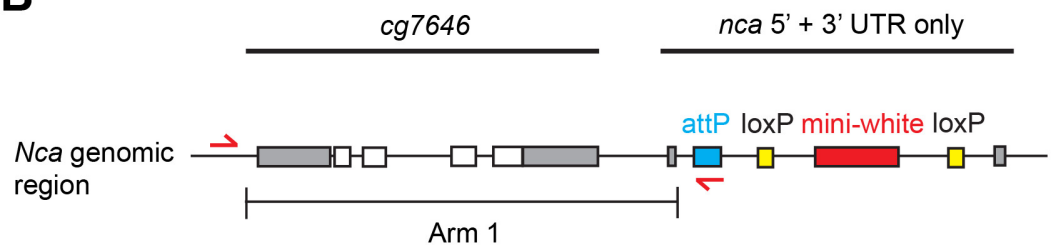

C

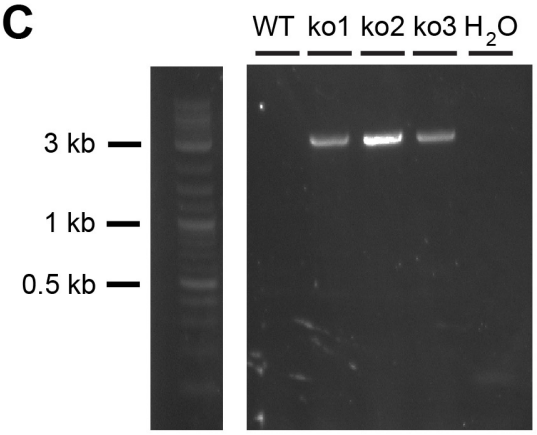

D

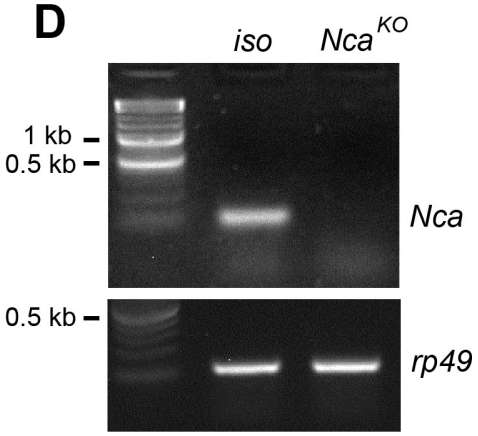

E

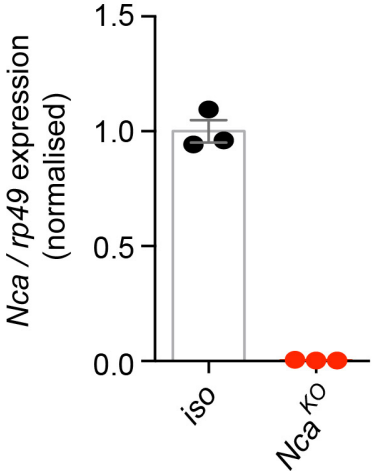

595

596 **Figure 1 supplemental figure 1.** Generation of the *Nca* knockout allele. (A)
597 Hippocalcin and Neurocalcin are highly conserved neuronal calcium sensors. Amino-
598 acid alignment of human (Hs) Hippocalcin (HPCA) and *Drosophila* (Dm)
599 Neurocalcin (NCA). Identical amino-acids are shaded in black, with functionally
600 similar amino-acids shaded in grey. Total homology between Hippocalcin and
601 Neurocalcin is > 90%. (B-C) PCR validation of homologous recombination events.
602 Correct recombination was verified using primers designed to the attP site and
603 upstream of the neighbouring locus *cg7646* (B), which will only generate a ~ 3 kb
604 product following homologous recombination between the targeting vector and the
605 *Nca* locus (C). Three independent targeting events (ko1-3) are shown in (C), one of
606 which was selected for mini-*white* removal as described in Figure 1. WT: wild-type
607 genome lacking an attP site neighbouring the *cg7646* locus. (D-E) No *Nca* mRNA
608 was detected in Nca^{KO} using either standard RT-PCR (D) or quantitative RT-PCR (E;
609 n = 3 qPCR reactions for *iso31* control and Nca^{KO} flies).
610
611

Figure 1 figure supplement 2

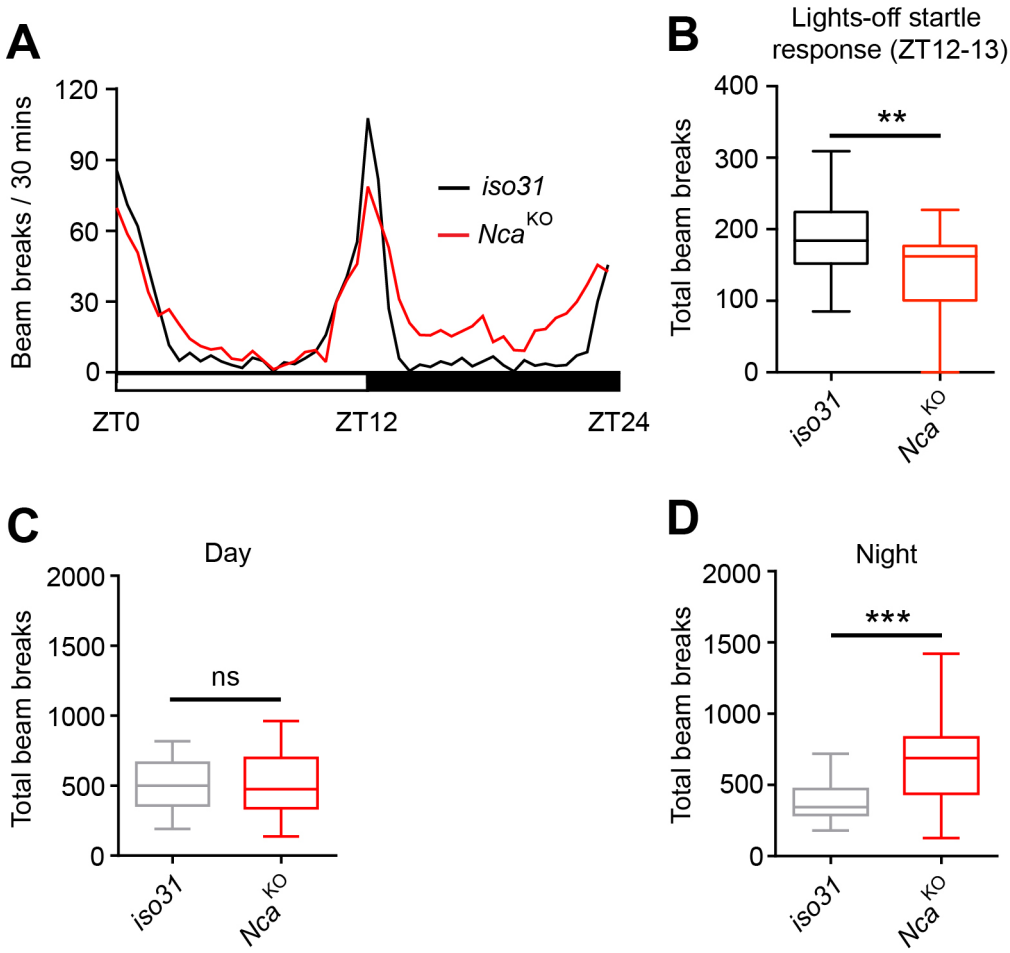

Figure 1 supplemental figure 2. Reduced startle response and elevated night time locomotor activity in *Nca*^{KO} flies. (A) Mean level of locomotor activity (beam crosses) for *iso31* control and *Nca*^{KO} males under 12L: 12D conditions. (B) Median beam breaks during the hour immediately following lights-off (ZT12-13). The rapid light-dark transition initiates a startle response and thus elevated locomotor activity, the degree of which is reduced in *Nca*^{KO} males. (C-D) Median total beam crosses during the day (C) and night (D) periods. Locomotor activity is significantly increased in *Nca*^{KO} males during the night but not the day. n = 32 per genotype. **$p < 0.01$, ***$p < 0.001$, ns – $p > 0.05$, Mann-Whitney U-test.

Figure 1 figure supplement 3

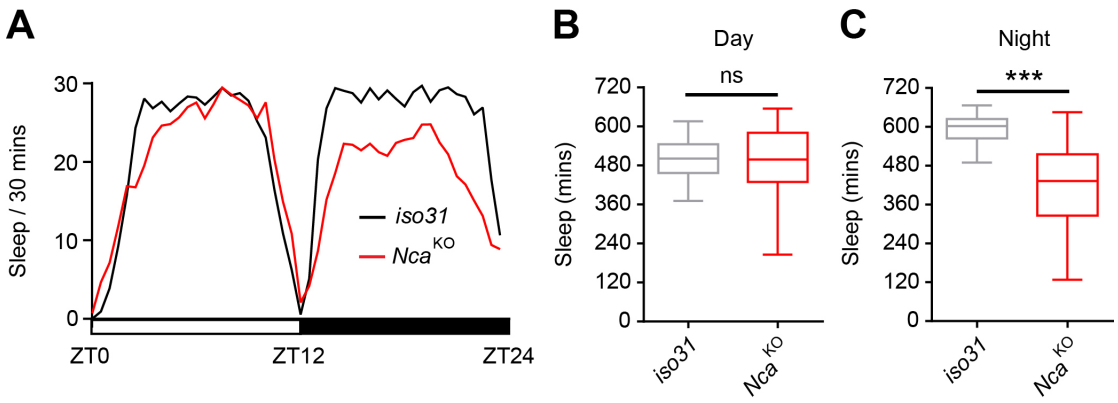

Figure 1 supplemental figure 3. Night time sleep loss in *Nca*^{KO} flies. (A) Mean sleep level of *iso31* control and *Nca*^{KO} flies under 12L: 12D conditions. (B-C) Median total day (B) and night (C) sleep in *iso31* control and *Nca*^{KO} flies. Night sleep is significantly reduced in *Nca*^{KO} flies compared to controls. n = 32 per genotype. ***$p < 0.001$, ns – $p > 0.05$, Mann-Whitney U-test.

Figure 1 figure supplement 4

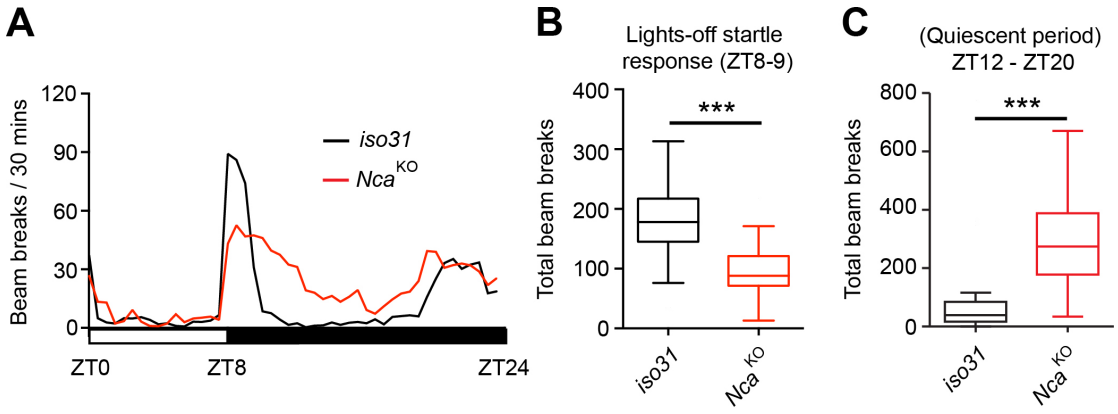

632

633

634 **Figure 1 supplemental figure 4.** Reduced startle response and elevated night time

635 locomotor activity in *Nca*^{KO} flies under 8L: 16D conditions. (A) Mean level of

636 locomotor activity (beam crosses) for *iso31* control and *Nca*^{KO} males. (B) Median

637 beam breaks during the hour immediately following lights-off (ZT8-9). (C-D) Median

638 total beam crosses during the normally quiescent period of the night (ZT12-20). n =

639 16 per genotype. ***$p < 0.001$, Mann-Whitney U-test.

640

641

642

Figure 1 figure supplement 5

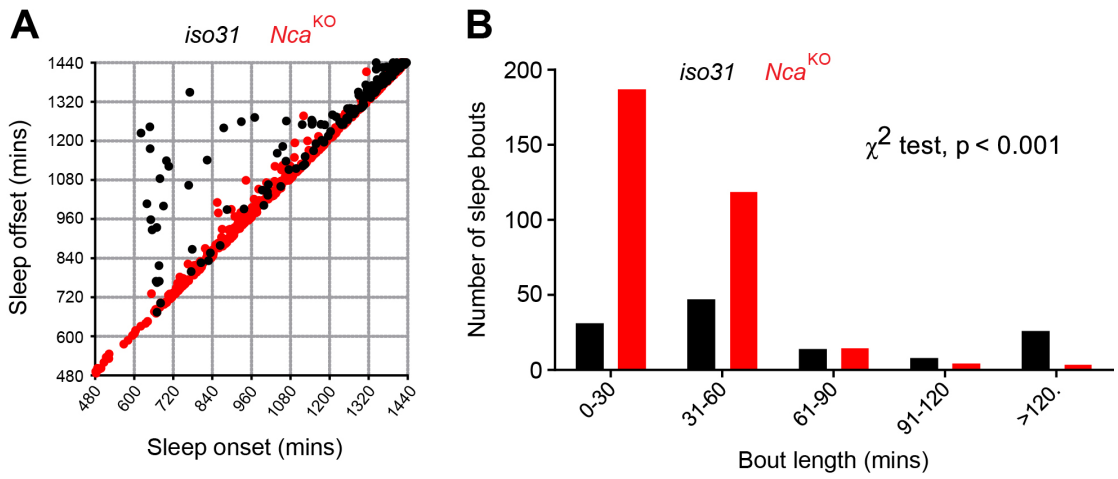

Figure 1 supplemental figure 5. Reduced long sleep bouts in *Nca*^{KO} flies. (A) Following detailed fly movement detection using the DART system, individual sleep bout durations were further estimated using a custom-made R program and visualised by plotting sleep bout offset against onset for night sleep bouts in control *iso31* and *Nca*^{KO} adult males under 8L: 16D conditions. In control flies, longer sleep bouts initiated early during the night (note the black dots deviating from the diagonal), which are largely absent in *Nca*^{KO} adult males (red dots). n = 16 for each genotype. (B) Distribution of sleep bout lengths in *Nca*^{KO} and control adult males. Note the significant shift towards shorter sleep bout lengths in *Nca*^{KO} flies (*Nca*^{KO} vs. *iso31* control: χ^2, *df*: 85.59, 4, $p < 0.001$).

Figure 1 figure supplement 6

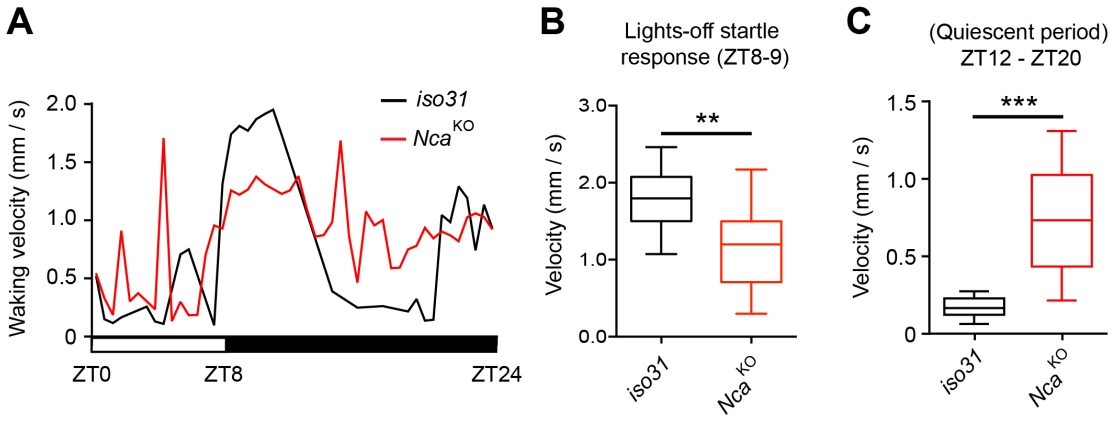

Figure 1 supplemental figure 6. Detailed tracking reveals increased locomotor velocity during the night and reduced velocity during the startle response to lights-off in *Nca*^{KO} flies. (A) Mean waking locomotor velocity in *iso31* control and *Nca*^{KO} adult males under L8: 16D condition. (B) Locomotor velocity is significantly reduced in *Nca*^{KO} flies following the startle response to lights-off (ZT8-ZT9). (C) *Nca*^{KO} flies exhibit a significant increase in locomotor velocity between ZT12-ZT20 compared to controls – a normally quiescent period. n = 16 per genotype. **$p < 0.01$, ***$p < 0.001$, Mann-Whitney U-test.

Figure 2

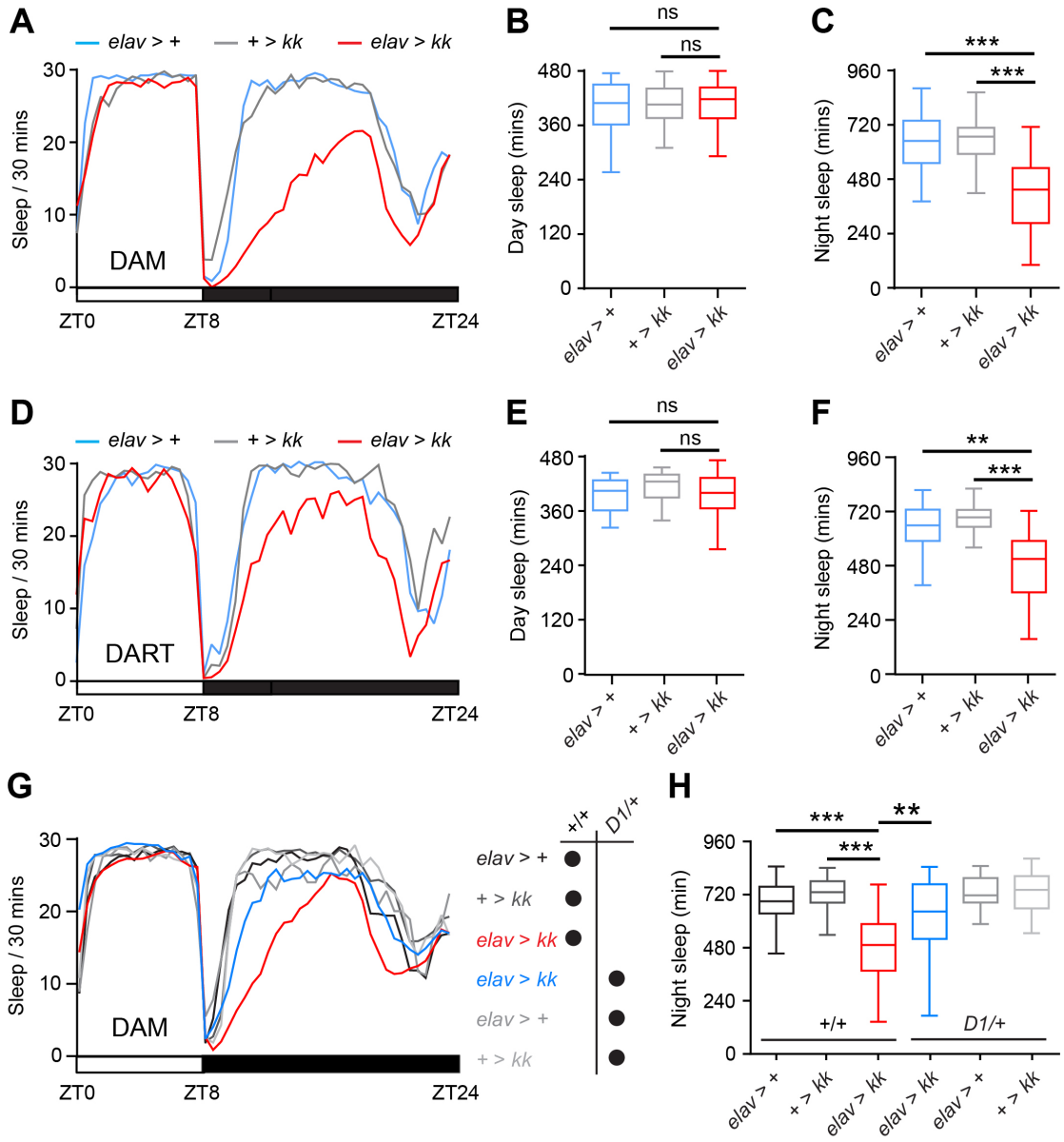

670

671

672 **Figure 2.** *Nca* and *Dop1R1* act in a common pathway to regulate night sleep. (A)

673 Mean sleep levels measured using the DAM system under 8L: 16D conditions for

674 pan-neuronal *Nca* knockdown (Nca^{KD}) male adult flies (*elav* > *kk*) and associated

675 controls (*elav*-Gal4 driver or *kk* RNAi transgene heterozygotes). (B-C) Median day

676 and night sleep levels in the above genotypes. n = 54-55. (D) Mean sleep levels

677 measured using DART system in 8L: 16D conditions for above genotypes. (E-F)

678 Median day and night sleep levels in the above genotypes. n = 20 per genotype. (G-H)
679 heterozygosity for the null or strongly hypomorphic Dop1R1 allele *Dop1R1*$^{MI03085-}$
680 $^{GFST.2}$ (*D1*/+) suppressed sleep loss in *Nca*^{KD} adult males, but did not alter sleep in
681 control males ($p > 0.05$, between +/+ and *D1*/+ backgrounds for *elav* > + or + > *kk*
682 flies). Mean sleep patterns in 8L: 16D conditions are shown in (G). Median total night
683 sleep levels are shown in (H). *elav* > *kk, D1*/+: n = 32; *elav* > +*, D1*/+: n = 15; + >
684 *kk, D1*/+: n = 32; *elav* > *kk*: n = 48*; elav* > +: n = 47; + > *kk*: n = 48. **$p < 0.01$,
685 ***$p < 0.001$, ns – $p < 0.05$, Kruskal-Wallis test with Dunn's post-hoc test.
686
687

Figure 2 figure supplement 1

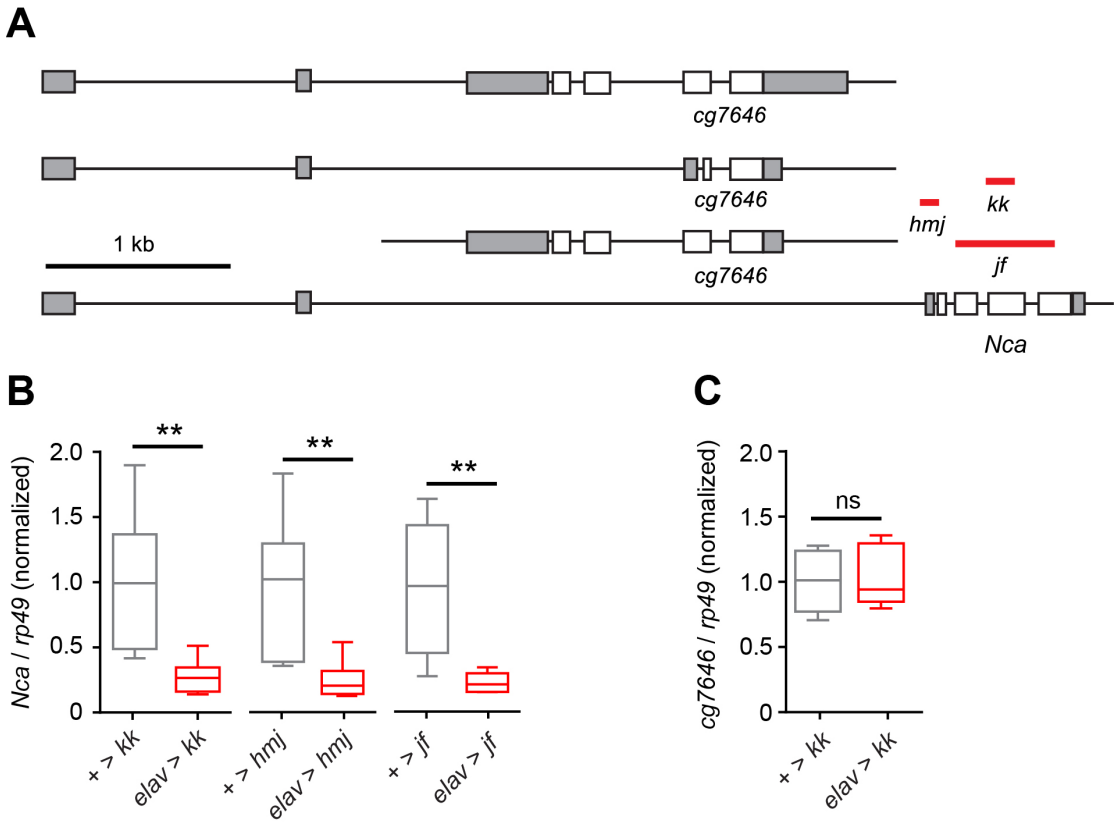

688

689

690 **Figure 2 supplemental figure 1.** Robust knockdown of *Nca* using independent *elav*-

691 Gal4-driven *Nca* RNAi lines. (A) Schematic showing the *Nca* locus alongside the

692 neighbouring *cg7646* locus, which shares a common promoter region with *Nca*.

693 Regions of the *Nca* transcript targeted by the *kk108825*, *hmj21533* and *jf03398* RNAi

694 lines (termed *kk*, *hmj* and *jf* respectively) are depicted by red bars. (B) qPCR

695 verification of *Nca* knockdown by *kk*, *hmj* and *jf*. RNAi. Transgene insertions lacking

696 the *elav*-Gal4 driver were used as controls. (C) Knockdown of *Nca* had no effect on

697 transcription of the neighbouring *cg7646* locus. Expression levels of *Nca* or *cg7646*

698 were normalised to the *rp49* control transcript and are displayed as the ratio to the

699 mean level of the respective RNAi alone controls (+ > *kk*, + > *hmj* or + > *jf*). n = 6 for

700 all qPCRs (two independent biological repetitions of RNA extraction with triplicated

701 qPCR reactions for each genotype). **$p < 0.01$, ns – $p > 0.05$, Mann-Whitney U-test.

702

Figure 2 figure supplement 2

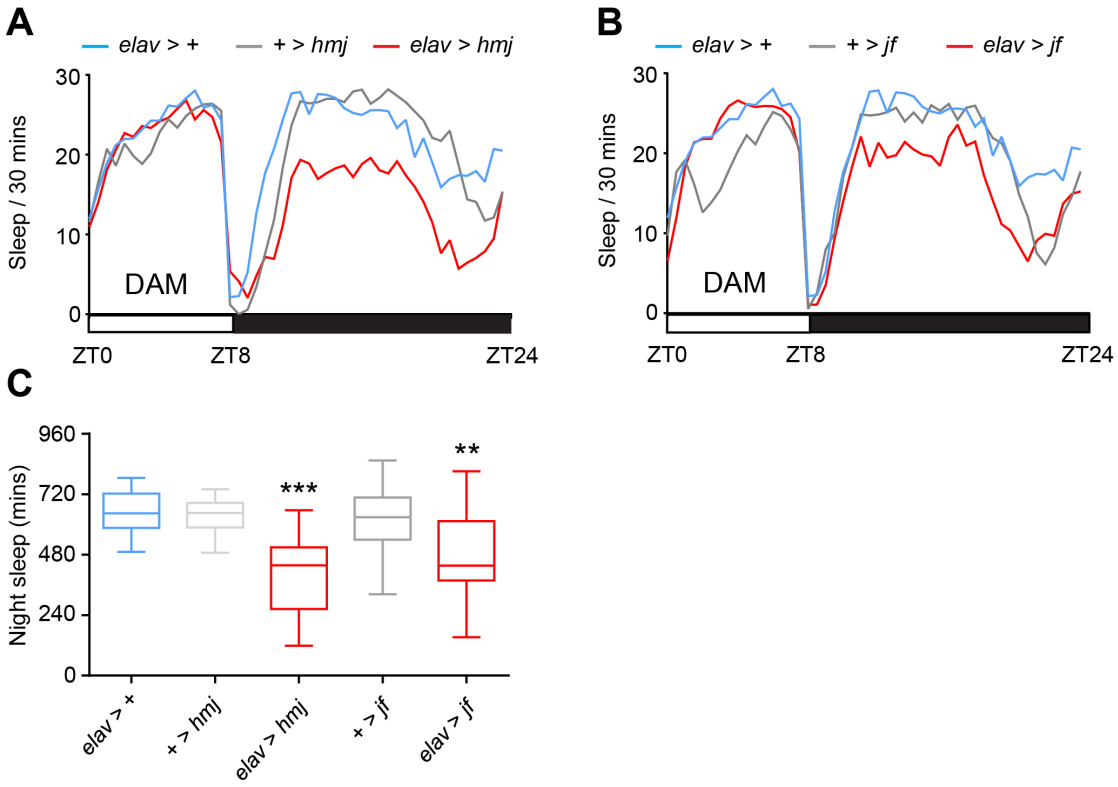

703

704

705 **Figure 2 supplemental figure 2.** Robust night sleep loss in adult male flies

706 expressing two independent *Nca* RNAi lines *driven by elav*-Gal4. (A-B) Mean sleep

707 profiles under 8L: 16D conditions for *elav*-gal4 drive, *hmj* (A) or *jf* (B) *Nca* RNAi.

708 (C) Median night sleep amounts for genotypes shown in (A-B). *elav* > +: n = 32; + >

709 *hmj*: n = 26; *elav* > *hmj*: n = 17; + > *jf*: n = 32; *elav* > *jf*: n = 32. **p < 0.01, ***p <

710 0.001 as compared to driver and RNAi alone controls, Kruskal-Wallis test with

711 Dunn's post-hoc test.

712

Figure 2 figure supplement 3

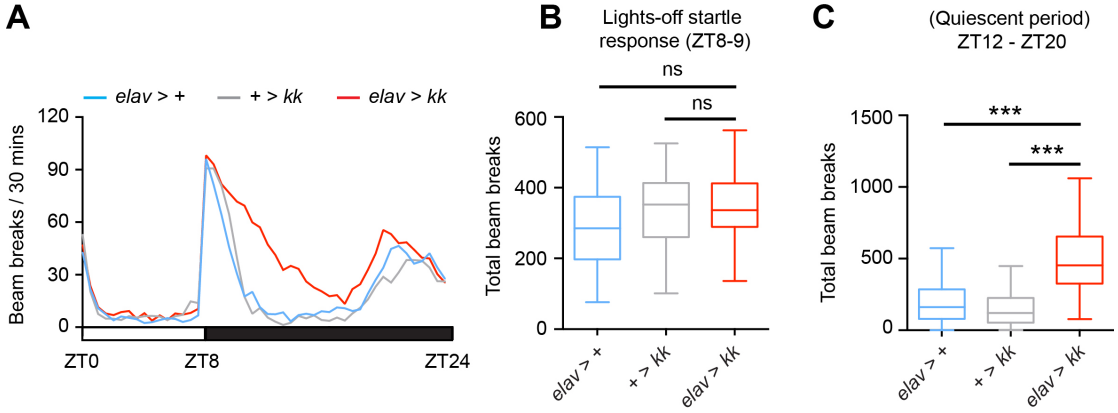

Figure 2 supplemental figure 3. Elevated night time locomotor activity in *Nca*^{KD} flies under 8L: 16D conditions, but no alteration in peak locomotor activity. (A) Mean level of locomotor activity (beam crosses) for *Nca*^{KD} males (*elav* > *kk*) and associated controls. (B) Median beam breaks during the hour immediately following lights-off (ZT8-9) in the above genotypes. (C) Median total beam crosses during the normally quiescent period of the night (ZT12-20) in the above genotypes. n = 54-55 per genotype. ***$p < 0.001$, ns – $p > 0.05$, Mann-Whitney U-test.

Figure 2 figure supplement 4

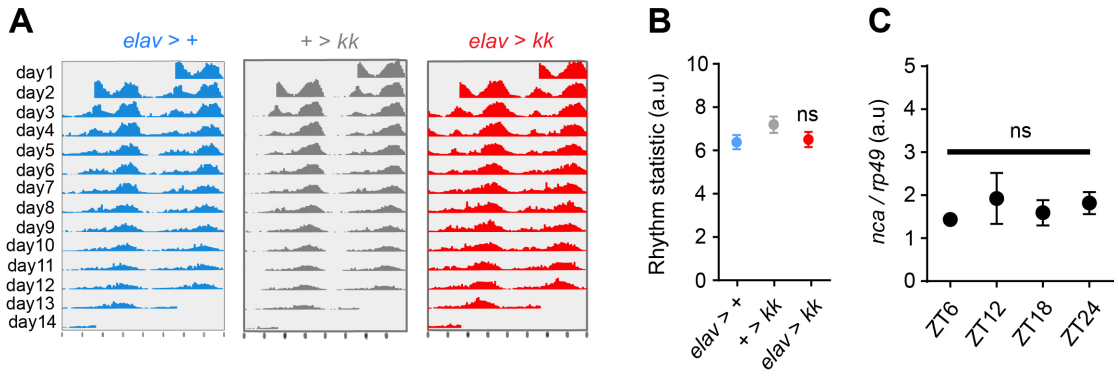

Figure 2 supplemental figure 4. *Nca* knockdown does not alter circadian rhythmicity. (A) Actograms showing representative individual patterns of locomotor activity across two weeks under constant dark conditions. (B) Quantification of locomotor rhythm strength. Robust circadian patterns of locomotor activity were still observed following in adult males expressing *Nca* RNAi (*kk*) under *elav*-Gal4 relative to controls. 15 > n > 14. (C) qPCR analysis of wild type (*Canton-S*) head *Nca* expression across a 24 h period. No evidence of circadian oscillations in *Nca* expression was observed. n = 3 (triplicated qPCR reactions for each time point). Expression levels were normalised to the *rp49* control transcript. ns – p > 0.05, Kruskal-Wallis test with Dunn's post-hoc test.

Figure 2 figure supplement 5

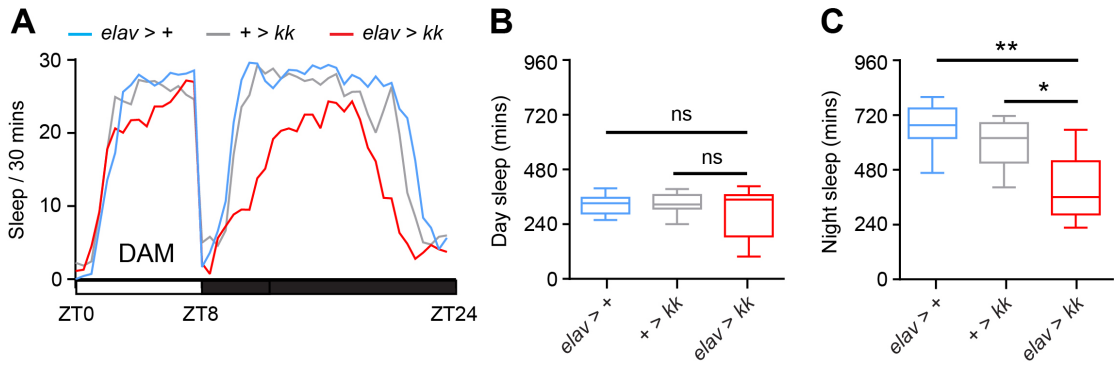

Figure 2 supplemental figure 5. Neuronal *Nca* knockdown results in reduced night sleep in adult virgin female *Drosophila*. (A) Mean sleep patterns of neuronal *Nca* knockdown females (*elav* > *kk*) and associated controls under 8L:16D conditions. (B-C) Median day sleep is unaffected relative to controls (B), whereas median night sleep is significantly reduced (C). n = 16 per genotype. *p < 0.05, **p < 0.01, Kruskal-Wallis test with Dunn's post-hoc test.

Figure 2 figure supplement 6

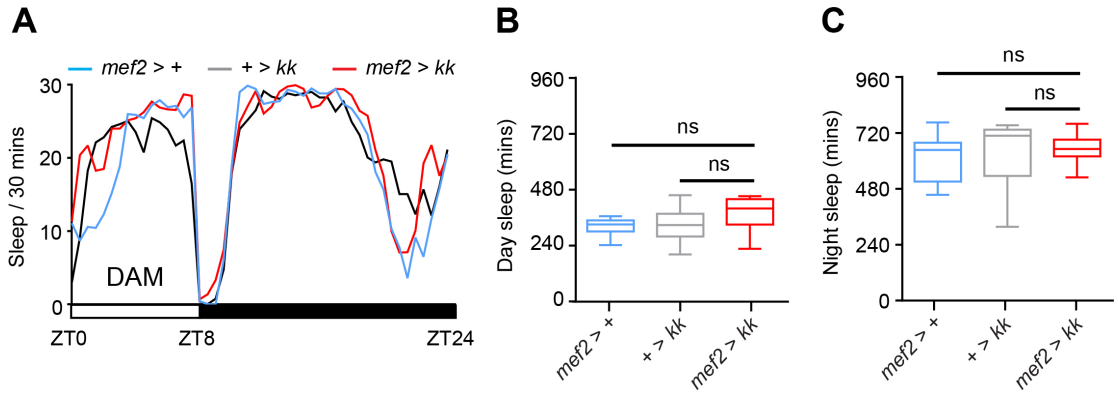

Figure 2 supplemental figure 6. *Nca* knockdown in muscle cells does not affect sleep in *Drosophila*. (A) Mean sleep patterns of adult male flies with muscle-specific *Nca* knockdown via *mef2*-Gal4 (*mef2* > *kk*) and associated controls under 8L: 16D. (B-C) Median day (B) and night (C) sleep levels are unaffected relative to controls. n = 16 per genotype. ns – $p > 0.05$, Kruskal-Wallis test with Dunn's post-hoc test.

Figure 2 figure supplement 7

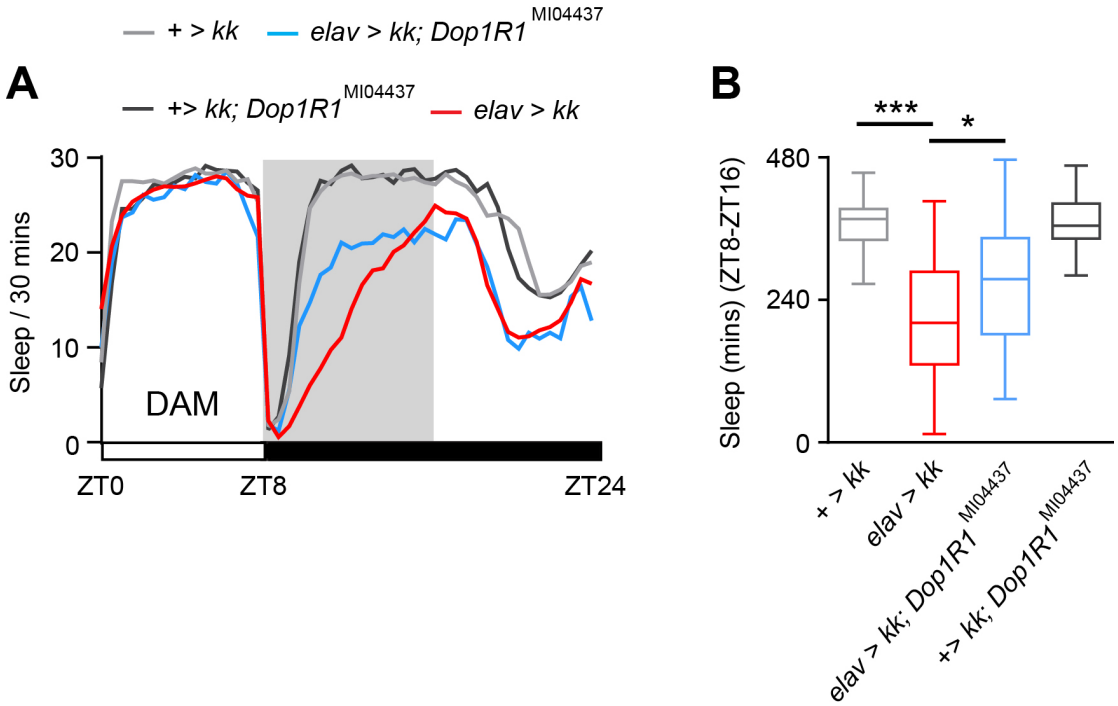

Figure 2 supplemental figure 7. Genetic interaction between *Nca* and a second independent *Dop1R1 allele*. (A) Mean sleep patterns of Nca^{KD} males (*elav* > *kk*) and a heterozygous *kk* alone control with and without one copy of the $Dop1R1^{MI04437}$ allele under 8L: 16D conditions. $Dop1R1^{MI04437}$ is a hypomorphic allele of Dop1R1 that is homozygous viable, and is therefore weaker compared to the homozygous lethal $Dop1R1^{MI03085\text{-}GFST.2}$ insertion. (B) Median night sleep levels during ZT8-16 are shown. Heterozygosity for $Dop1R1^{MI04437}$ had no impact on sleep in *kk* heterozygote controls but partially rescued night sleep during ZT8-16 in Nca^{KD} males. *elav* > *kk*: n = 64; + > *kk*: n = 64; *elav* > *kk*; $Dop1R1^{MI04437}$/+: n = 39; + > *kk*; $Dop1R1^{MI04437}$/+: n = 45. *p < 0.05, ***p < 0.001, Kruskal-Wallis test with Dunn's post-hoc test.

Figure 2 figure supplement 8

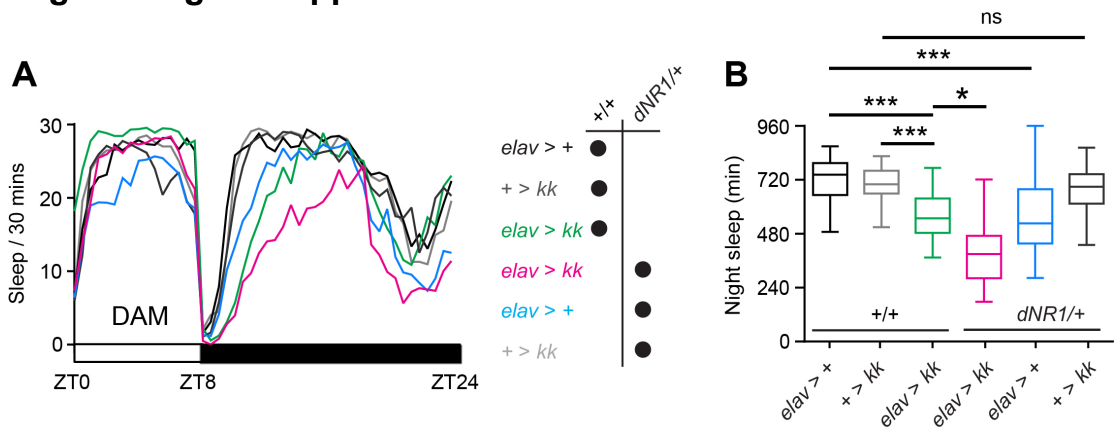

Figure 2 supplemental figure 8. NCA regulate sleeps in a distinct pathway to the dNR1 NMDA receptor. (A) Mean sleep patterns of *Nca*^{KD} males (*elav* > *kk*) and heterozygous controls with and without one copy of the *dNR1*^{MI11796} (*dNR1*/+) allele in 8L: 16D conditions are shown. (B) Median night sleep levels in the above genotypes. Heterozygosity for *dNR1*^{MI11796} resulted in sleep loss in *elav*-Gal4 driver controls, and reduced sleep further in an additive manner in *elav* > *kk Nca*^{KD} males, suggesting that NCA and dNR1 act in separate pathways to promote night sleep. *Elav* > *kk*; *dNR1*/+: n = 32; *elav* > +; *dNR1*/+: n = 26; + > *kk*; *dNR1*/+: n = 38; *elav* > *kk*: n = 32; *elav* > +: n = 30; + > *kk*: n = 34. ns – p > 0.05, *p < 0.05, **p < 0.01, ***p < 0.001, Kruskal-Wallis test with Dunn's post-hoc test.

Figure 3

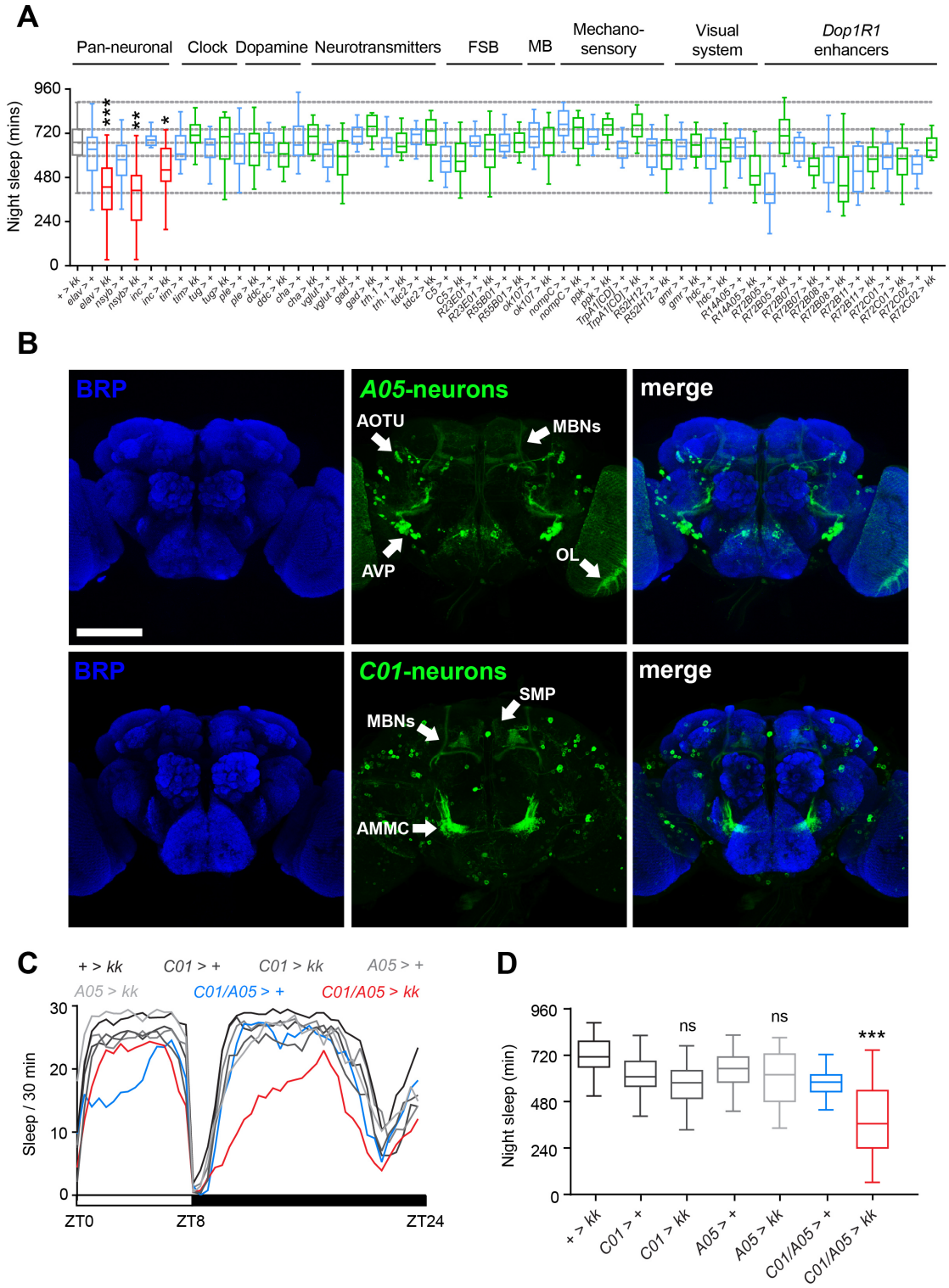

Figure 3. NCA acts in a two distinct neural networks to regulate night sleep. (A) Transgenic RNAi-based mini-screen to identify key NCA-expressing neurons. NCA

788 knockdown with broadly expressed drivers resulted in reduced night sleep in adult
789 males under 8L: 16D conditions. In contrast, NCA knockdown in previously defined
790 sleep-regulatory centers, clock neurons, the visual system or subsets of Dop1R1-
791 expressing neurons did not impact night sleep. FSB: fan-shaped body. MB:
792 mushroom body. Grey and blue box plots: control lines. Red box plots: experimental
793 lines showing reduced night sleep relative to controls. Green box plots: experimental
794 lines failing to show reduced night sleep relative to one or both controls. See Figure 3
795 figure supplement 1 for n-values and statistical comparisons. (B) Confocal z-stacks of
796 adult male brains expressing genetically-encoded fluorophores under the *A05* or *C01*-
797 Gal4 drivers. Neuropil regions are labelled with anti-Bruchpilot (BRP). Scale bar =
798 100 µm. Arrows point to neuropil centers. AOTU: anterior optic tubercle. MBNs:
799 mushroom body neurons. OL: optic lobe. AMMC: antennal mechanosensory and
800 motor center. AVP: anterior ventrallateral protocerebrum. SMP: supra-medial
801 protocerebrum. (C-D) *Nca* knockdown in both *A05* and *C01*-neurons recapitulates the
802 effect of pan-neuronal *Nca* knockdown, whereas *Nca* knockdown in either neuronal
803 subpopulation alone did not reduce sleep relative to controls. Mean sleep patterns in
804 8L: 16D conditions are shown in (C). Median night sleep levels are shown in (D). + >
805 *kk*: n = 80; *C01* > +: n = 64, *C01* > *kk*: n = 80; *A05* > +: n = 31; *A05* > *kk*: n = 31;
806 *C01/A05* > +: n = 42; *C01/A05* > *kk*: n = 71. *p < 0.05, **p < 0.01, ***p < 0.001, ns
807 – p > 0.05 compared to driver and RNAi alone controls, Kruskal-Wallis test with
808 Dunn's post-hoc test.
809

Figure 3 figure supplement 1. Night sleep levels in flies with *kk Nca RNAi* driven by neuron sub-type-specific Gal4 drivers.

Genotype	n-values	25% Percentile (min)	Median (min)	75% Percentile (min)	Mean (min)	Std. Deviation (min)	Dunn's test vs +>kk	vs Gal4 >+
+>kk	275	602	671	742	668	110	-	-
elav>+	86	518	633	698	604	133	-	-
elav>kk	99	306	428	530	413	168	***	***
nsyb>+	40	491	576	654	565	121	-	-
nsyb>kk	39	248	409	490	388	196	***	*
inc>+	14	655	684	705	688	56	-	-
inc>kk	30	460	521	637	534	128	***	**
tim>+	16	577	607	707	636	91	-	-
tim>kk	16	668	709	767	707	80	ns	ns
tug>+	16	590	658	688	650	117	-	-
tug>kk	15	580	701	805	670	134	ns	ns
ple>+	32	556	663	718	634	132	-	-
ple>kk	30	545	670	718	642	101	ns	ns
Ddc>+	16	616	658	721	662	63	-	-
Ddc>kk	16	538	608	667	610	84	ns	ns
Chat>+	16	601	656	758	677	111	-	-
Chat>kk	14	607	704	766	672	140	ns	ns
vGlut>+	16	536	632	660	607	91	-	-
vGlut>kk	24	495	594	679	586	111	ns	ns
GAD>+	16	662	703	752	689	82	-	-
GAD>kk	16	705	758	817	739	100	ns	ns
Trh.1>+	16	598	635	696	640	83	-	-
Trh.1>kk	16	617	649	720	668	71	ns	ns
Tdc2>+	16	659	715	742	682	105	-	-
Tdc2>kk	15	657	733	794	695	128	ns	ns
C5>+	40	509	568	648	583	103	-	-
C5>kk	49	513	567	665	581	107	***	ns
R23E10>+	16	651	670	705	680	48	-	-
R23E10>kk	16	535	632	712	621	122	ns	ns
R55B01>+	16	621	653	714	652	107	-	-
R55B01>kk	16	618	670	721	680	80	ns	ns
OK107>+	23	644	702	777	695	94	-	-

OK107>kk	32	601	668	751	664	106	ns	ns
nompC>+	16	708	769	842	768	76	-	-
nompC>kk	16	638	753	804	725	92	ns	ns
ppk>+	16	661	701	742	706	62	-	-
ppk>kk	16	712	766	798	760	78	ns	ns
trpACD>+	16	586	639	677	630	62	-	-
trpACD>kk	15	702	764	825	758	75	ns	*
R52H12>+	16	536	654	689	629	92	-	-
R52H12>kk	32	525	603	684	581	155	ns	ns
GMR>+	16	582	649	685	640	73	-	-
GMR>kk	14	592	656	714	652	79	ns	ns
Hdc>+	16	527	599	694	575	145	-	-
Hdc>kk	16	566	641	686	624	86	ns	ns
R21G01>+	15	584	646	694	631	75	-	-
R21G01>kk	16	440	489	598	519	109	**	ns
R72B05>+	15	341	388	502	397	146	-	-
R72B05>kk	16	611	706	795	710	107	ns	***
R72B07>+	13	570	668	697	645	66	-	-
R72B07>kk	14	492	541	585	545	69	**	ns
R72B08>+	16	452	595	643	561	129	-	-
R72B08>kk	32	348	436	591	474	159	***	ns
R72B11>+	16	403	515	651	513	123	-	-
R72B11>kk	15	512	580	645	583	88	ns	ns
R72C01>+	48	528	590	662	591	84	-	-
R72C01>kk	64	496	582	639	569	104	***	ns
R72C02>+	16	500	551	595	544	62	-	-
R72C02>kk	16	591	627	694	643	60	ns	ns

- Not significant, ns-p>0.05, *p < 0.05, **p < 0.01, ***p < 0.001, Kruskal-Wallis test with Dunn's post-hoc test.

Figure 3 figure supplement 2

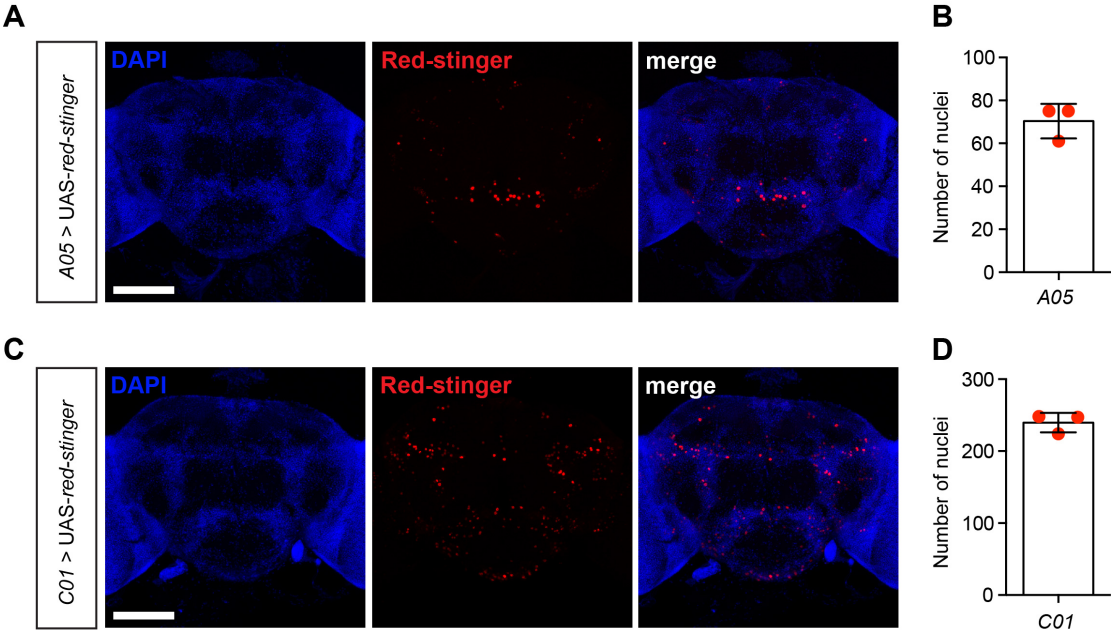

Figure 3 supplemental figure 2. *C01*-Gal4 and *A05*-Gal4 label small subsets of neurons in the adult fly brain. (A, C) Representative confocal z-stacks of adult male brains expressing nuclear RFP marker (Red-stinger) under *A05*-Gal4 (A) or *C01*-Gal4 driver (C). DAPI-staining labels nuclei within the *Drosophila* brain. (B, D) Number of cells expressing Red-stinger driven by *A05*- (B) or *C01*-Gal4 (D). n = 3 for each genotype. Scale bar =100 μm.

Figure 3 figure supplement 3

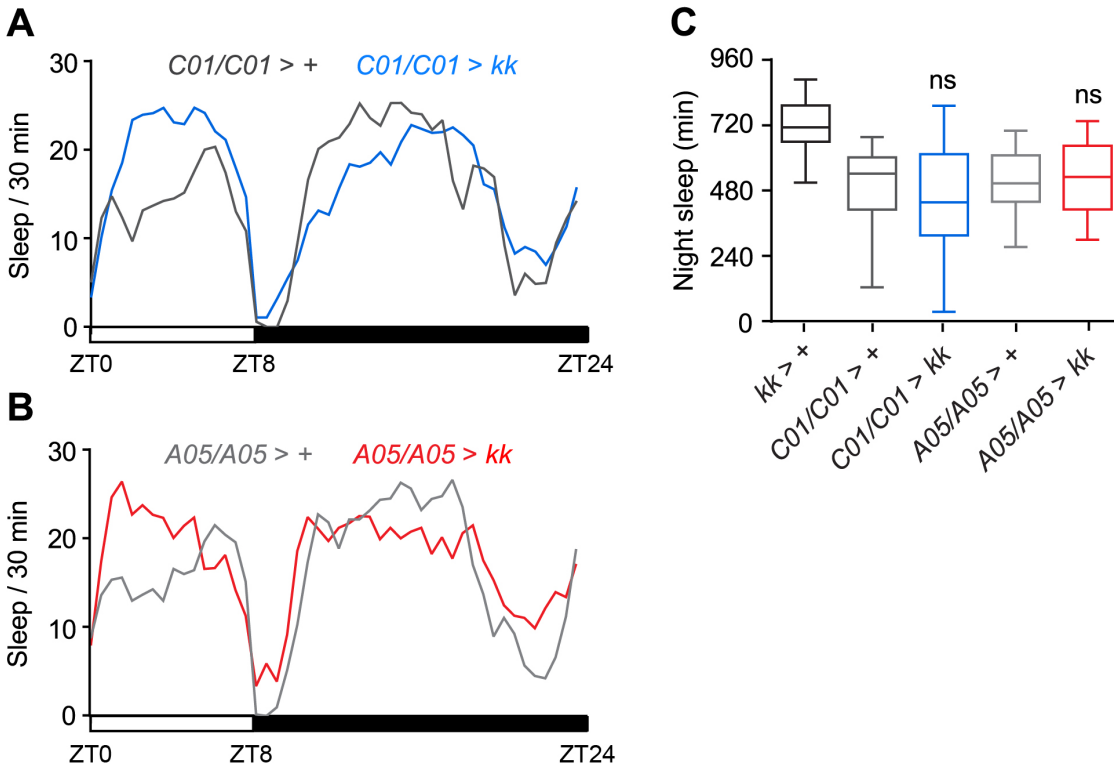

Figure 3 supplemental figure 3. (A) Mean sleep patterns of adult males homozygous for the *C01*-Gal4 driver with and without the *kk Nca* RNAi insertion. (B) Mean sleep patterns of adult males homozygous for the *A05*-Gal4 driver with and without the *kk Nca* RNAi insertion. (C) Median night sleep levels for heterozygous RNAi transgene and homozygous driver controls, and males expressing *Nca* RNAi with two Gal4 driver copies. No night sleep loss was observed using two copies of either driver relative to controls. + > *kk*: n = 80 (the same population was used in Figure 3C, as the experiments were performed side by side), *C01/C01* > +: n = 24, *C01/C01* > *kk*: n = 39; *A05/A05* > : n = 22, *A05/A05* > *kk*: n = 23. ns – p > 0.05, Kruskal-Wallis test with Dunn's post-hoc test.

Figure 3 figure supplement 4

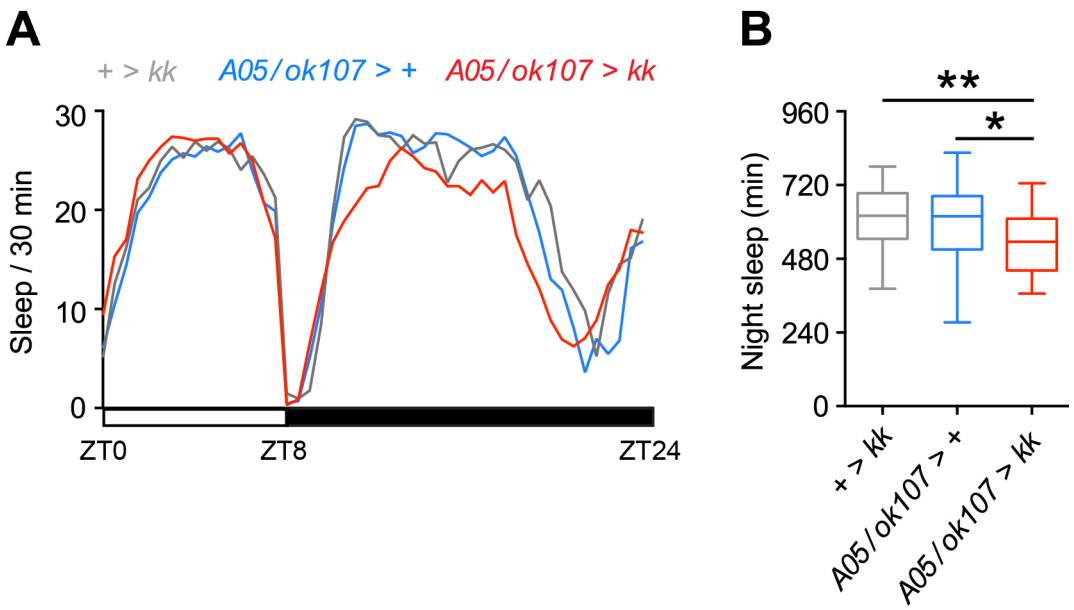

Figure 3 supplemental figure 4. Knockdown of *Nca* in mushroom body and *A05*-neurons results in partial night sleep loss. (A-B) *Nca* knockdown in both *A05* and MB-neurons (defined by *ok107*-Gal4; *ok107*) results in reduced night sleep (also see Figure 3A showing *ok107* > *kk* alone does not cause night sleep loss). Mean sleep patterns in 8L: 16D conditions are shown in (A). Median night sleep levels are shown in (B). + > *kk*: n = 31; *A05/ok107* > +: n = 33; *A05/ok107* > *kk*: n = 42. *p < 0.05, **p < 0.01, Kruskal-Wallis test with Dunn's post-hoc test.

Figure 4

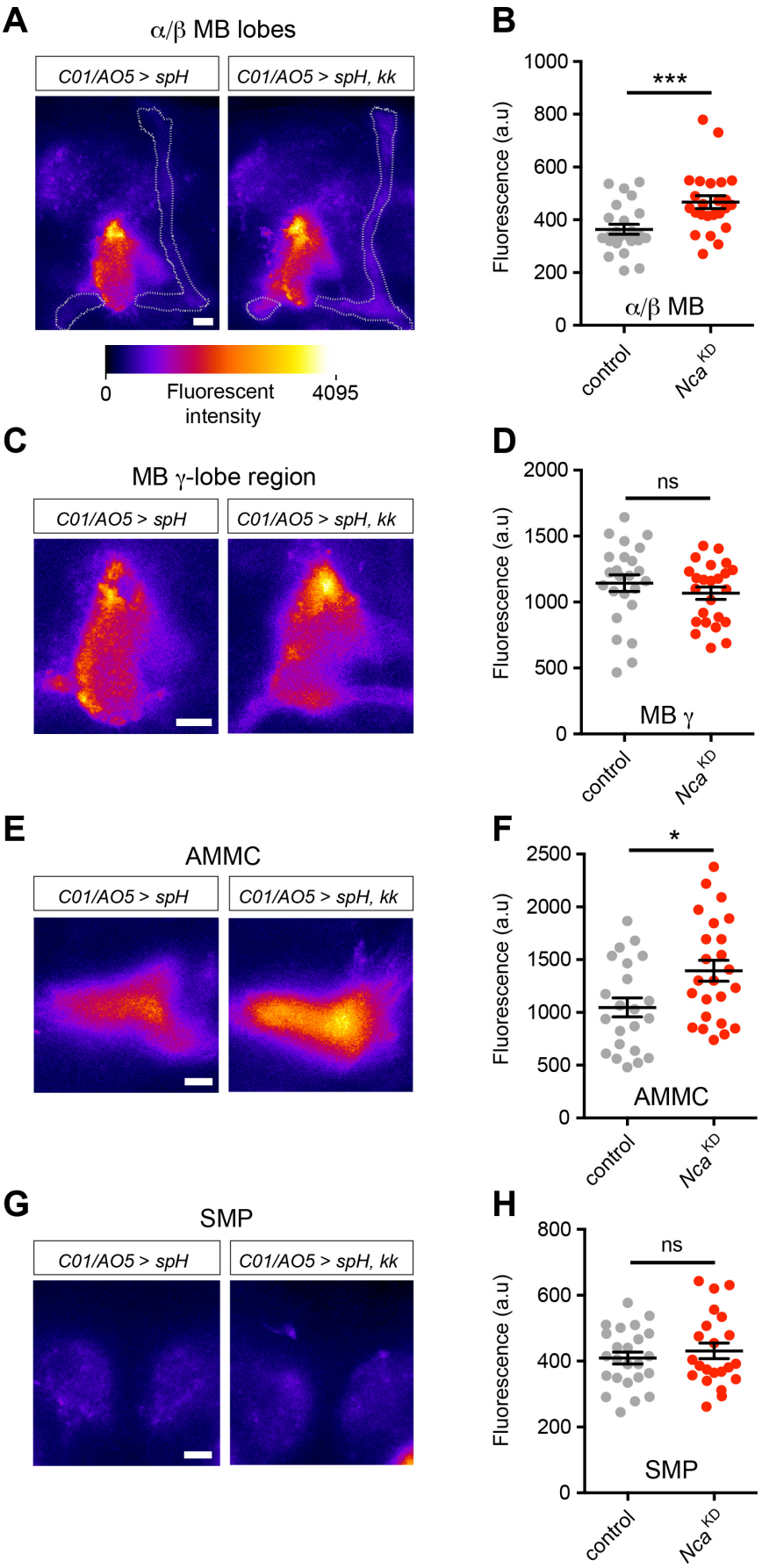
A
α/β MB lobes
C01/AO5 > spH
C01/AO5 > spH, kk
0
Fluorescent intensity
4095
B
***
Fluorescence (a.u)
1000
800
600
400
200
0
α/β MB
control
Nca KD
C
MB γ-lobe region
C01/AO5 > spH
C01/AO5 > spH, kk
D
ns
Fluorescence (a.u)
2000
1500
1000
500
0
MB γ
control
Nca KD
E
AMMC
C01/AO5 > spH
C01/AO5 > spH, kk
F
*
Fluorescence (a.u)
2500
2000
1500
1000
500
0
AMMC
control
Nca KD
G
SMP
C01/AO5 > spH
C01/AO5 > spH, kk
H
ns
Fluorescence (a.u)
800
600
400
200
0
SMP
control
Nca KD

851

852 **Figure 4.** NCA inhibits synaptic release in subsets of *C01*/*A05* neurons. Expression of
853 a fluorescent marker for synaptic release (synapto-pHluorin, spH) in *C01*- and *A05*-
854 positive neurons in control (*C01*/*A05* > *spH*) or *Nca* knockdown (*C01/A05* > *spH, kk*)
855 backgrounds. Adult brains were dissected and imaged between ZT9-ZT11, when
856 robust sleep loss occurs in *C01*/*A05* > *kk* flies (see Figure 3C). (A, C, E, G)
857 Representative pseudo-coloured images for α/β mushroom body lobe Kenyon cells
858 (α/β MB, A; α/β lobes are outlined in white), the MB γ-lobe region (C), AMMC (E)
859 and SMP (G) regions in each genotype. Fluorescent intensity range is shown in the
860 horizontal bar, illustrating minimum to maximum spectrum. Scale bars = 10 μm. (B,
861 D, F, H) Mean fluorescent intensity for individual hemispheres in the above regions. n
862 = 22-24. *$p < 0.05$, ***$p < 0.001$, Mann-Whitney U-test.
863
864

Figure 5

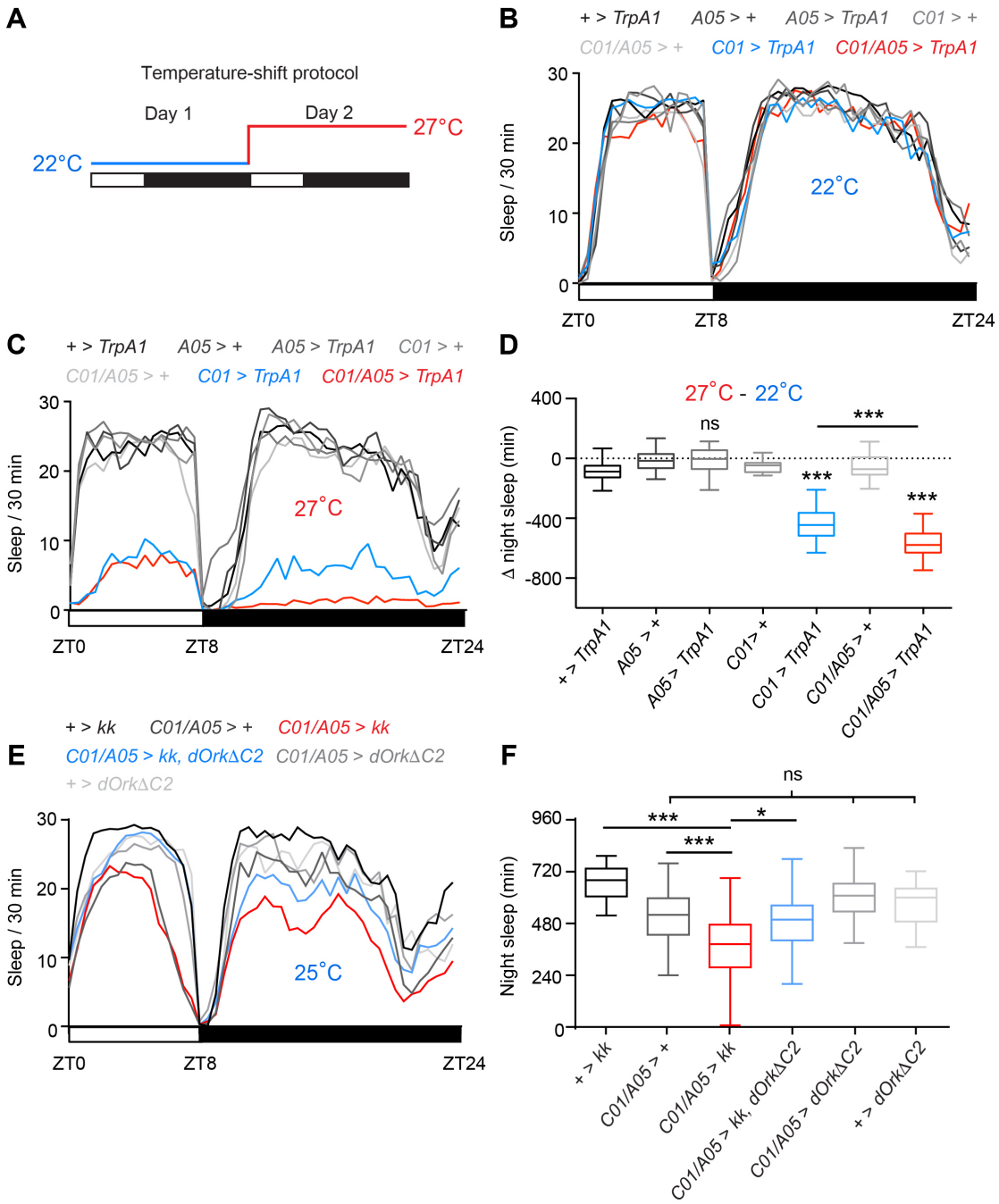

Figure 5. Sleep loss in *Nca* knockdown flies is caused by enhanced excitability of *C01/A05* neurons. (A) Experimental paradigm for acute activation of *A05* or *C01*-neurons. 22°C: non-activating temperature for TrpA1. 27°C: activating temperature. Sleep measurements were measured over two days in 8L: 16D conditions. (B-C) Mean sleep levels across 8L: 16D following expression of TrpA1 in *A05*-, *C01*- or

872 *A05*- and *C01*-neurons (and associated controls) at 22°C (B) or 27°C (C). (D) Median
873 change in night sleep levels (Δ night sleep) following the shift from 22°C on day 1 to
874 27°C on day 2. + > *TrpA1*: n = 53; *A05* > +: n = 23; *A05* > *TrpA1*: n = 68; *C01* > +: n
875 = 24; *C01* > *TrpA1*: n = 40; *C01/A05* > +: n = 33; *C01/A05* > *TrpA1*: n = 40. ***p <
876 0.001, ns – p > 0.05, as compared to *TrpA1* or driver alone controls by Kruskal-Wallis
877 test with Dunn's post-hoc test (for *C01, A05* or *C01/ A05* > *TrpA1* compared to
878 controls) or Mann-Whitney U-test (for *C01/A05* > *TrpA1* compared to *C01* > *TrpA1*).
879 (E-F) Inhibition of *C01/A05* neurons by expressing dORKΔC2 rescues sleep loss due
880 to *Nca* knockdown in *C01/A05* neurons, while expression of dORKΔC2 does not
881 change base line sleep. Mean sleep patterns in 8L: 16D conditions are shown in (E).
882 Median night sleep levels are shown in (F). +> *kk*: n = 47, *C01/A05* >+: n = 47,
883 *C01/A05* > *kk*: n = 62, *C01/A05* > *dORKΔC2, kk*: n = 50, *C01/A05* > *dORKΔC2*: n =
884 39, + > *dORKΔC2*: n = 30. *p < 0.05, ***p < 0.001, ns – p > 0.05, Kruskal-Wallis
885 test with Dunn's post-hoc test.
886
887
888
889
890
891
892
893
894
895

896 **References**

897 Afonso, D.J., Liu, D., Machado, D.R., Pan, H., Jepson, J.E., Rogulja, D., and Koh, K.
898 (2015). TARANIS Functions with Cyclin A and Cdk1 in a Novel Arousal Center to
899 Control Sleep in *Drosophila*. Curr Biol *25*, 1717-1726.

900 Andrade, R., Foehring, R.C., and Tzingounis, A.V. (2012). The calcium-activated
901 slow AHP: cutting through the Gordian knot. Front Cell Neurosci *6*, 47.

902 Baena-Lopez, L.A., Alexandre, C., Mitchell, A., Pasakarnis, L., and Vincent, J.P.
903 (2013). Accelerated homologous recombination and subsequent genome modification
904 in *Drosophila*. Development *140*, 4818-4825.

905 Braunewell, K.H., and Klein-Szanto, A.J. (2009). Visinin-like proteins (VSNLs):
906 interaction partners and emerging functions in signal transduction of a subfamily of
907 neuronal Ca2+ -sensor proteins. Cell Tissue Res *335*, 301-316.

908 Breakefield, X.O., Blood, A.J., Li, Y., Hallett, M., Hanson, P.I., and Standaert, D.G.
909 (2008). The pathophysiological basis of dystonias. Nat Rev Neurosci *9*, 222-234.

910 Burgoyne, R.D., and Haynes, L.P. (2012). Understanding the physiological roles of
911 the neuronal calcium sensor proteins. Mol Brain *5*, 2.

912 Calabresi, P., Pisani, A., Rothwell, J., Ghiglieri, V., Obeso, J.A., and Picconi, B.
913 (2016). Hyperkinetic disorders and loss of synaptic downscaling. Nat Neurosci *19*,
914 868-875.

915 Charlesworth, G., Angelova, P.R., Bartolome-Robledo, F., Ryten, M., Trabzuni, D.,
916 Stamelou, M., Abramov, A.Y., Bhatia, K.P., and Wood, N.W. (2015). Mutations in
917 HPCA cause autosomal-recessive primary isolated dystonia. Am J Hum Genet *96*,
918 657-665.

919 Charlesworth, G., Plagnol, V., Holmstrom, K.M., Bras, J., Sheerin, U.M., Preza, E.,
920 Rubio-Agusti, I., Ryten, M., Schneider, S.A., Stamelou, M.*, et al.* (2012). Mutations

921 in ANO3 cause dominant craniocervical dystonia: ion channel implicated in
922 pathogenesis. Am J Hum Genet *91*, 1041-1050.
923 Donlea, J.M., Thimgan, M.S., Suzuki, Y., Gottschalk, L., and Shaw, P.J. (2011).
924 Inducing sleep by remote control facilitates memory consolidation in *Drosophila*.
925 Science *332*, 1571-1576.
926 Fahn, S. (1988). Concept and classification of dystonia. Adv Neurol *50*, 1-8.
927 Faville, R., Kottler, B., Goodhill, G.J., Shaw, P.J., and van Swinderen, B. (2015).
928 How deeply does your mutant sleep? Probing arousal to better understand sleep
929 defects in *Drosophila*. Sci Rep *5*, 8454.
930 Fuchs, T., Gavarini, S., Saunders-Pullman, R., Raymond, D., Ehrlich, M.E.,
931 Bressman, S.B., and Ozelius, L.J. (2009). Mutations in the THAP1 gene are
932 responsible for DYT6 primary torsion dystonia. Nat Genet *41*, 286-288.
933 Fuchs, T., Saunders-Pullman, R., Masuho, I., Luciano, M.S., Raymond, D., Factor, S.,
934 Lang, A.E., Liang, T.W., Trosch, R.M., White, S.*, et al.* (2013). Mutations in GNAL
935 cause primary torsion dystonia. Nat Genet *45*, 88-92.
936 Gerfen, C.R., and Surmeier, D.J. (2011). Modulation of striatal projection systems by
937 dopamine. Annu Rev Neurosci *34*, 441-466.
938 Hamada, F.N., Rosenzweig, M., Kang, K., Pulver, S.R., Ghezzi, A., Jegla, T.J., and
939 Garrity, P.A. (2008). An internal thermal sensor controlling temperature preference in
940 *Drosophila*. Nature *454*, 217-220.
941 Helassa, N., Antonyuk, S.V., Lian, L.Y., Haynes, L.P., and Burgoyne, R.D. (2017).
942 Biophysical and functional characterization of hippocalcin mutants responsible for
943 human dystonia. Hum Mol Genet *26*: 2426-2435.

944 Jenett, A., Rubin, G.M., Ngo, T.T., Shepherd, D., Murphy, C., Dionne, H., Pfeiffer,
945 B.D., Cavallaro, A., Hall, D., Jeter, J.*, et al.* (2012). A GAL4-driver line resource for
946 *Drosophila* neurobiology. Cell Rep *2*, 991-1001.
947 Jiang, Y., Pitmon, E., Berry, J., Wolf, F.W., McKenzie, Z., and Lebestky, T.J. (2016).
948 A Genetic Screen To Assess Dopamine Receptor (DopR1) Dependent Sleep
949 Regulation in *Drosophila*. G3 (Bethesda) *6*, 4217-4226.
950 Jo, J., Son, G.H., Winters, B.L., Kim, M.J., Whitcomb, D.J., Dickinson, B.A., Lee,
951 Y.B., Futai, K., Amici, M., Sheng, M.*, et al.* (2010). Muscarinic receptors induce
952 LTD of NMDAR EPSCs via a mechanism involving hippocalcin, AP2 and PSD-95.
953 Nat Neurosci *13*, 1216-1224.
954 Joiner, W.J., Crocker, A., White, B.H., and Sehgal, A. (2006). Sleep in *Drosophila* is
955 regulated by adult mushroom bodies. Nature *441*, 757-760.
956 Kamikouchi, A., Inagaki, H.K., Effertz, T., Hendrich, O., Fiala, A., Göpfert, M.C.,
957 and Ito, K. (2009). The neural basis of *Drosophila* gravity-sensing and hearing.
958 Nature *458*, 165-171.
959 Karimi, M., and Perlmutter, J.S. (2015). The role of dopamine and dopaminergic
960 pathways in dystonia: insights from neuroimaging. Tremor Other Hyperkinet Mov (N
961 Y) *5*, 280.
962 Kume, K., Kume, S., Park, S.K., Hirsh, J., and Jackson, F.R. (2005). Dopamine is a
963 regulator of arousal in the fruit fly. J Neurosci *25*, 7377-7384.
964 Lamaze, A., Ozturk-Colak, A., Fischer, R., Peschel, N., Koh, K., and Jepson, J.E.
965 (2017). Regulation of sleep plasticity by a thermo-sensitive circuit in *Drosophila*. Sci
966 Rep *7*, 40304.
967 Lebestky, T., Chang, J.S., Dankert, H., Zelnik, L., Kim, Y.C., Han, K.A., Wolf, F.W.,
968 Perona, P., and Anderson, D.J. (2009). Two different forms of arousal in *Drosophila*

969 are oppositely regulated by the dopamine D1 receptor ortholog DopR via distinct
970 neural circuits. Neuron *64*, 522-536.
971 Lee, H.J., Weitz, A.J., Bernal-Casas, D., Duffy, B.A., Choy, M., Kravitz, A.V.,
972 Kreitzer, A.C., and Lee, J.H. (2016). Activation of Direct and Indirect Pathway
973 Medium Spiny Neurons Drives Distinct Brain-wide Responses. Neuron *91*, 412-424.
974 Lehner, B. (2013). Genotype to phenotype: lessons from model organisms for human
975 genetics. Nat Rev Genet *14*, 168-178.
976 Levine, J.D., Funes, P., Dowse, H.B., and Hall, J.C. (2002a). Advanced analysis of a
977 cryptochrome mutation's effects on the robustness and phase of molecular cycles in
978 isolated peripheral tissues of *Drosophila*. BMC neuroscience *3*, 5.
979 Levine, J.D., Funes, P., Dowse, H.B., and Hall, J.C. (2002b). Signal analysis of
980 behavioral and molecular cycles. BMC neuroscience *3*, 1.
981 Li, Q., Kellner, D.A., Hatch, H.A.M., Yumita, T., Sanchez, S., Machold, R.P., Frank,
982 C.A., and Stavropoulos, N. (2017). Conserved properties of *Drosophila insomniac*
983 link sleep regulation and synaptic function. PLoS Genet *13*, e1006815.
984 Liu, Q., Liu, S., Kodama, L., Driscoll, M.R., and Wu, M.N. (2012). Two
985 dopaminergic neurons signal to the dorsal fan-shaped body to promote wakefulness in
986 *Drosophila*. Curr Biol *22*, 2114-2123.
987 Liu, S., Lamaze, A., Liu, Q., Tabuchi, M., Yang, Y., Fowler, M., Bharadwaj, R.,
988 Zhang, J., Bedont, J., Blackshaw, S.*, et al.* (2014). WIDE AWAKE mediates the
989 circadian timing of sleep onset. Neuron *82*, 151-166.
990 McGary, K.L., Park, T.J., Woods, J.O., Cha, H.J., Wallingford, J.B., and Marcotte,
991 E.M. (2010). Systematic discovery of nonobvious human disease models through
992 orthologous phenotypes. Proc Natl Acad Sci U S A *107*, 6544-6549.

993 Mencacci, N.E., Rubio-Agusti, I., Zdebik, A., Asmus, F., Ludtmann, M.H., Ryten,
994 M., Plagnol, V., Hauser, A.K., Bandres-Ciga, S., Bettencourt, C.*, et al.* (2015). A
995 missense mutation in KCTD17 causes autosomal dominant myoclonus-dystonia. Am
996 J Hum Genet *96*, 938-947.
997 Miesenbock, G. (2012). Synapto-pHluorins: genetically encoded reporters of synaptic
998 transmission. Cold Spring Harb Protoc *2012*, 213-217.
999 Nitabach, M.N., Blau, J., and Holmes, T.C. (2002). Electrical silencing of *Drosophila*
1000 pacemaker neurons stops the free-running circadian clock. Cell *109*, 485-495.
1001 Pappas, S.S., Darr, K., Holley, S.M., Cepeda, C., Mabrouk, O.S., Wong, J.M., LeWitt,
1002 T.M., Paudel, R., Houlden, H., Kennedy, R.T.*, et al.* (2015). Forebrain deletion of the
1003 dystonia protein torsinA causes dystonic-like movements and loss of striatal
1004 cholinergic neurons. Elife *4*, e08352.
1005 Park, D., and Griffith, L.C. (2006). Electrophysiological and anatomical
1006 characterization of PDF-positive clock neurons in the intact adult *Drosophila* brain. J
1007 Neurophysiol *95*, 3955-3960.
1008 Peterson, D.A., Sejnowski, T.J., and Poizner, H. (2010). Convergent evidence for
1009 abnormal striatal synaptic plasticity in dystonia. Neurobiol Dis *37*, 558-573.
1010 Pfeiffenberger, C., and Allada, R. (2012). Cul3 and the BTB adaptor insomniac are
1011 key regulators of sleep homeostasis and a dopamine arousal pathway in *Drosophila*.
1012 PLoS Genet *8*, e1003003.
1013 Pfeiffenberger, C., Lear, B.C., Keegan, K.P., and Allada, R. (2010a). Locomotor
1014 activity level monitoring using the *Drosophila* Activity Monitoring (DAM) System.
1015 Cold Spring Harb Protoc *2010*, pdb prot5518.

1016 Pfeiffenberger, C., Lear, B.C., Keegan, K.P., and Allada, R. (2010b). Processing sleep
1017 data created with the *Drosophila* Activity Monitoring (DAM) System. Cold Spring
1018 Harb Protoc *2010*, pdb prot5520.
1019 Pitman, J.L., McGill, J.J., Keegan, K.P., and Allada, R. (2006). A dynamic role for
1020 the mushroom bodies in promoting sleep in *Drosophila*. Nature *441*, 753-756.
1021 Rogulja, D., and Young, M.W. (2012). Control of sleep by cyclin A and its regulator.
1022 Science *335*, 1617-1621.
1023 Seidner, G., Robinson, J.E., Wu, M., Worden, K., Masek, P., Roberts, S.W., Keene,
1024 A.C., and Joiner, W.J. (2015). Identification of Neurons with a Privileged Role in
1025 Sleep Homeostasis in *Drosophila melanogaster*. Curr Biol *25*, 2928-2938.
1026 Shi, M., Yue, Z., Kuryatov, A., Lindstrom, J.M., and Sehgal, A. (2014). Identification
1027 of Redeye, a new sleep-regulating protein whose expression is modulated by sleep
1028 amount. Elife *3*, e01473.
1029 Sitaraman, D., Aso, Y., Jin, X., Chen, N., Felix, M., Rubin, G.M., and Nitabach, M.N.
1030 (2015). Propagation of Homeostatic Sleep Signals by Segregated Synaptic
1031 Microcircuits of the *Drosophila* Mushroom Body. Curr Biol *25*, 2915-2927.
1032 Stavropoulos, N., and Young, M.W. (2011). insomniac and Cullin-3 regulate sleep
1033 and wakefulness in Drosophila. Neuron *72*, 964-976.
1034 Tanabe, L.M., Kim, C.E., Alagem, N., and Dauer, W.T. (2009). Primary dystonia:
1035 molecules and mechanisms. Nat Rev Neurol *5*, 598-609.
1036 Tecuapetla, F., Jin, X., Lima, S.Q., and Costa, R.M. (2016). Complementary
1037 Contributions of Striatal Projection Pathways to Action Initiation and Execution. Cell
1038 *166*, 703-715.

1039 Teng, D.H., Chen, C.K., and Hurley, J.B. (1994). A highly conserved homologue of
1040 bovine neurocalcin in *Drosophila melanogaster* is a Ca(2+)-binding protein expressed
1041 in neuronal tissues. J Biol Chem *269*, 31900-31907.
1042 Tomita, J., Ban, G., and Kume, K. (2017). Genes and neural circuits for sleep of the
1043 fruit fly. Neurosci Res *118*, 82-91.
1044 Tomita, J., Ueno, T., Mitsuyoshi, M., Kume, S., and Kume, K. (2015). The NMDA
1045 Receptor Promotes Sleep in the Fruit Fly, *Drosophila melanogaster*. PLoS One *10*,
1046 e0128101.
1047 Tzingounis, A.V., Kobayashi, M., Takamatsu, K., and Nicoll, R.A. (2007).
1048 Hippocalcin gates the calcium activation of the slow afterhyperpolarization in
1049 hippocampal pyramidal cells. Neuron *53*, 487-493.
1050 Ueno, K., Naganos, S., Hirano, Y., Horiuchi, J., and Saitoe, M. (2013). Long-term
1051 enhancement of synaptic transmission between antennal lobe and mushroom body in
1052 cultured *Drosophila* brain. J Physiol *591*, 287-302.
1053 Ueno, T., Tomita, J., Tanimoto, H., Endo, K., Ito, K., Kume, S., and Kume, K. (2012).
1054 Identification of a dopamine pathway that regulates sleep and arousal in *Drosophila*.
1055 Nat Neurosci *15*, 1516-1523.
1056 Wakabayashi-Ito, N., Ajjuri, R.R., Henderson, B.W., Doherty, O.M., Breakefield,
1057 X.O., O'Donnell, J.M., and Ito, N. (2015). Mutant human torsinA, responsible for
1058 early-onset dystonia, dominantly suppresses GTPCH expression, dopamine levels and
1059 locomotion in *Drosophila melanogaster*. Biol Open *4*, 585-595.
1060 Wakabayashi-Ito, N., Doherty, O.M., Moriyama, H., Breakefield, X.O., Gusella, J.F.,
1061 O'Donnell, J.M., and Ito, N. (2011). Dtorsin, the *Drosophila* ortholog of the early-
1062 onset dystonia TOR1A (DYT1), plays a novel role in dopamine metabolism. PLoS
1063 One *6*, e26183.

1064 Weisheit, C.E., and Dauer, W.T. (2015). A novel conditional knock-in approach
1065 defines molecular and circuit effects of the DYT1 dystonia mutation. Hum Mol Genet
1066 *24*, 6459-6472.
1067 Wenning, G.K., Kiechl, S., Seppi, K., Muller, J., Hogl, B., Saletu, M., Rungger, G.,
1068 Gasperi, A., Willeit, J., and Poewe, W. (2005). Prevalence of movement disorders in
1069 men and women aged 50-89 years (Bruneck Study cohort): a population-based study.
1070 Lancet Neurol *4*, 815-820.
1071 Wu, M., Robinson, J.E., and Joiner, W.J. (2014). SLEEPLESS is a bifunctional
1072 regulator of excitability and cholinergic synaptic transmission. Curr Biol *24*, 621-629.
1073 Yokoi, F., Dang, M.T., Liu, J., Gandre, J.R., Kwon, K., Yuen, R., and Li, Y. (2015).
1074 Decreased dopamine receptor 1 activity and impaired motor-skill transfer in Dyt1
1075 DeltaGAG heterozygous knock-in mice. Behav Brain Res *279*, 202-210.
1076 Zhong, L., Bellemer, A., Yan, H., Ken, H., Jessica, R., Hwang, R.Y., Pitt, G.S., and
1077 Tracey, W.D. (2012). Thermosensory and nonthermosensory isoforms of *Drosophila*
1078 *melanogaster* TRPA1 reveal heat-sensor domains of a thermoTRP Channel. Cell Rep
1079 *1*, 43-55.
1080
1081